Eur. Phys. J. C 10, 373–393 (1999)
Digital Object Identifier (DOI) 10.1007/s100529900138

THE EUROPEAN PHYSICAL JOURNAL C

Charmonium production in deep inelastic scattering at HERA

The H1 Collaboration

C. Adloff[34], V. Andreev[25], B. Andrieu[28], V. Arkadov[35], A. Astvatsatourov[35], I. Ayyaz[29], A. Babaev[24], J. Bähr[35], P. Baranov[25], E. Barrelet[29], W. Bartel[11], U. Bassler[29], P. Bate[22], A. Beglarian[11,40], O. Behnke[11], H.-J. Behrend[11], C. Beier[15], A. Belousov[25], Ch. Berger[1], G. Bernardi[29], T. Berndt[15], G. Bertrand-Coremans[4], P. Biddulph[22], J.C. Bizot[27], V. Boudry[28], W. Braunschweig[1], V. Brisson[27], D.P. Brown[22], W. Brückner[13], P. Bruel[28], D. Bruncko[17], J. Bürger[11], F.W. Büsser[12], A. Buniatian[32], S. Burke[18], A. Burrage[19], G. Buschhorn[26], D. Calvet[23], A.J. Campbell[11], T. Carli[26], E. Chabert[23], M. Charlet[4], D. Clarke[5], B. Clerbaux[4], J.G. Contreras[8,43], C. Cormack[19], J.A. Coughlan[5], M.-C. Cousinou[23], B.E. Cox[22], G. Cozzika[10], J. Cvach[30], J.B. Dainton[19], W.D. Dau[16], K. Daum[39], M. David[10], M. Davidsson[21], A. De Roeck[11], E.A. De Wolf[4], B. Delcourt[27], R. Demirchyan[11,40], C. Diaconu[23], M. Dirkmann[8], P. Dixon[20], W. Dlugosz[7], K.T. Donovan[20], J.D. Dowell[3], A. Droutskoi[24], J. Ebert[34], G. Eckerlin[11], D. Eckstein[35], V. Efremenko[24], S. Egli[37], R. Eichler[36], F. Eisele[14], E. Eisenhandler[20], E. Elsen[11], M. Enzenberger[26], M. Erdmann[14,42,f], A.B. Fahr[12], P.J.W. Faulkner[3], L. Favart[4], A. Fedotov[24], R. Felst[11], J. Feltesse[10], J. Ferencei[17], F. Ferrarotto[32], M. Fleischer[8], G. Flügge[2], A. Fomenko[25], J. Formánek[31], J.M. Foster[22], G. Franke[11], E. Gabathuler[19], K. Gabathuler[33], F. Gaede[26], J. Garvey[3], J. Gassner[33], J. Gayler[11], R. Gerhards[11], S. Ghazaryan[11,40], A. Glazov[35], L. Goerlich[6], N. Gogitidze[25], M. Goldberg[29], I. Gorelov[24], C. Grab[36], H. Grässler[2], T. Greenshaw[19], R.K. Griffiths[20], G. Grindhammer[26], T. Hadig[1], D. Haidt[11], L. Hajduk[6], M. Hampel[1], V. Haustein[34], W.J. Haynes[5], B. Heinemann[11], G. Heinzelmann[12], R.C.W. Henderson[18], S. Hengstmann[37], H. Henschel[35], R. Heremans[4], I. Herynek[30], K. Hewitt[3], K.H. Hiller[35], C.D. Hilton[22], J. Hladký[30], D. Hoffmann[11], R. Horisberger[33], S. Hurling[11], M. Ibbotson[22], Ç. İşsever[8], M. Jacquet[27], M. Jaffre[27], L. Janauschek[26], D.M. Jansen[13], L. Jönsson[21], D.P. Johnson[4], M. Jones[19], H. Jung[21], H.K. Kästli[36], M. Kander[11], D. Kant[20], M. Kapichine[9], M. Karlsson[21], O. Karschnik[12], J. Katzy[11], O. Kaufmann[14], M. Kausch[11], N. Keller[14], I.R. Kenyon[3], S. Kermiche[23], C. Keuker[1], C. Kiesling[26], M. Klein[35], C. Kleinwort[11], G. Knies[11], J.H. Köhne[26], H. Kolanoski[38], S.D. Kolya[22], V. Korbel[11], P. Kostka[35], S.K. Kotelnikov[25], T. Krämerkämper[8], M.W. Krasny[29], H. Krehbiel[11], D. Krücker[26], K. Krüger[11], A. Küpper[34], H. Küster[2], M. Kuhlen[26], T. Kurča[35], W. Lachnit[11], R. Lahmann[11], D. Lamb[3], M.P.J. Landon[20], W. Lange[35], U. Langenegger[36], A. Lebedev[25], F. Lehner[11], V. Lemaitre[11], R. Lemrani[10], V. Lendermann[8], S. Levonian[11], M. Lindstroem[21], G. Lobo[27], E. Lobodzinska[6,41], V. Lubimov[24], S. Lüders[36], D. Lüke[8,11], L. Lytkin[13], N. Magnussen[34], H. Mahlke-Krüger[11], N. Malden[22], E. Malinovski[25], I. Malinovski[25], R. Maraček[17], P. Marage[4], J. Marks[14], R. Marshall[22], H.-U. Martyn[1], J. Martyniak[6], S.J. Maxfield[19], T.R. McMahon[19], A. Mehta[5], K. Meier[15], P. Merkel[11], F. Metlica[13], A. Meyer[11], A. Meyer[11], H. Meyer[34], J. Meyer[11], P.-O. Meyer[2], S. Mikocki[6], D. Milstead[11], R. Mohr[26], S. Mohrdieck[12], M.N. Mondragon[8], F. Moreau[28], A. Morozov[9], J.V. Morris[5], D. Müller[37], K. Müller[11], P. Murín[17], V. Nagovizin[24], B. Naroska[12], J. Naumann[8], Th. Naumann[35], I. Négri[23], P.R. Newman[3], H.K. Nguyen[29], T.C. Nicholls[11], F. Niebergall[12], C. Niebuhr[11], Ch. Niedzballa[1], H. Niggli[36], O. Nix[15], G. Nowak[6], T. Nunnemann[13], H. Oberlack[26], J.E. Olsson[11], D. Ozerov[24], P. Palmen[2], V. Panassik[9], C. Pascaud[27], S. Passaggio[36], G.D. Patel[19], H. Pawletta[2], E. Perez[10], J.P. Phillips[19], A. Pieuchot[11], D. Pitzl[36], R. Pöschl[8], G. Pope[7], B. Povh[13], K. Rabbertz[1], J. Rauschenberger[12], P. Reimer[30], B. Reisert[26], D. Reyna[11], H. Rick[11], S. Riess[12], E. Rizvi[3], P. Robmann[37], R. Roosen[4], K. Rosenbauer[1], A. Rostovtsev[24,12], F. Rouse[7], C. Royon[10], S. Rusakov[25], K. Rybicki[6], D.P.C. Sankey[5], P. Schacht[26], J. Scheins[1], F.-P. Schilling[14], S. Schleif[15], P. Schleper[14], D. Schmidt[34], D. Schmidt[11], L. Schoeffel[10], V. Schröder[11], H.-C. Schultz-Coulon[11], F. Sefkow[37], A. Semenov[24], V. Shekelyan[26], I. Sheviakov[25], L.N. Shtarkov[25], G. Siegmon[16], Y. Sirois[28], T. Sloan[18], P. Smirnov[25], M. Smith[19], V. Solochenko[24], Y. Soloviev[25], V. Spaskov[9], A. Specka[28], H. Spitzer[12], F. Squinabol[27], R. Stamen[8], P. Steffen[11], R. Steinberg[2], J. Steinhart[12], B. Stella[32], A. Stellberger[15], J. Stiewe[15], U. Straumann[14], W. Struczinski[2], J.P. Sutton[3], M. Swart[15], S. Tapprogge[15], M. Taševský[30], V. Tchernyshov[24], S. Tchetchelnitski[24], J. Theissen[2], G. Thompson[20], P.D. Thompson[3], N. Tobien[11], R. Todenhagen[13], D. Traynor[20], P. Truöl[37], G. Tsipolitis[36], J. Turnau[6], E. Tzamariudaki[26], S. Udluft[26], A. Usik[25], S. Valkár[31], A. Valkárová[31], C. Vallée[23], P. Van Esch[4], A. Van Haecke[10], P. Van Mechelen[4], Y. Vazdik[25], G. Villet[10], K. Wacker[8], R. Wallny[14], T. Walter[37], B. Waugh[22], G. Weber[12], M. Weber[15], D. Wegener[8], A. Wegner[26], T. Wengler[14], M. Werner[14], L.R. West[3], G. White[18], S. Wiesand[34], T. Wilksen[11], S. Willard[7], M. Winde[35], G.-G. Winter[11], Ch. Wissing[8], C. Wittek[12], E. Wittmann[13], M. Wobisch[2], H. Wollatz[11], E. Wünsch[11], J. Žáček[31], J. Zálešák[31], Z. Zhang[27], A. Zhokin[24], P. Zini[29], F. Zomer[27], J. Zsembery[10], M. zur Nedden[37]

[1] I. Physikalisches Institut der RWTH, Aachen, Germany[a]
[2] III. Physikalisches Institut der RWTH, Aachen, Germany[a]
[3] School of Physics and Space Research, University of Birmingham, Birmingham, UK[b]
[4] Inter-University Institute for High Energies ULB-VUB, Brussels; Universitaire Instelling Antwerpen, Wilrijk; Belgium[c]
[5] Rutherford Appleton Laboratory, Chilton, Didcot, UK[b]
[6] Institute for Nuclear Physics, Cracow, Poland[d]
[7] Physics Department and IIRPA, University of California, Davis, California, USA[e]
[8] Institut für Physik, Universität Dortmund, Dortmund, Germany[a]
[9] Joint Institute for Nuclear Research, Dubna, Russia
[10] DSM/DAPNIA, CEA/Saclay, Gif-sur-Yvette, France
[11] DESY, Hamburg, Germany[a]
[12] II. Institut für Experimentalphysik, Universität Hamburg, Hamburg, Germany[a]
[13] Max-Planck-Institut für Kernphysik, Heidelberg, Germany[a]
[14] Physikalisches Institut, Universität Heidelberg, Heidelberg, Germany[a]
[15] Institut für Hochenergiephysik, Universität Heidelberg, Heidelberg, Germany[a]
[16] Institut für experimentelle und angewandte Physik, Universität Kiel, Kiel, Germany[a]
[17] Institute of Experimental Physics, Slovak Academy of Sciences, Košice, Slovak Republic[f,j]
[18] School of Physics and Chemistry, University of Lancaster, Lancaster, UK[b]
[19] Department of Physics, University of Liverpool, Liverpool, UK[b]
[20] Queen Mary and Westfield College, London, UK[b]
[21] Physics Department, University of Lund, Lund, Sweden[g]
[22] Department of Physics and Astronomy, University of Manchester, Manchester, UK[b]
[23] CPPM, Université d'Aix-Marseille II, IN2P3-CNRS, Marseille, France
[24] Institute for Theoretical and Experimental Physics, Moscow, Russia
[25] Lebedev Physical Institute, Moscow, Russia[f,k]
[26] Max-Planck-Institut für Physik, München, Germany[a]
[27] LAL, Université de Paris-Sud, IN2P3-CNRS, Orsay, France
[28] LPNHE, École Polytechnique, IN2P3-CNRS, Palaiseau, France
[29] LPNHE, Universités Paris VI and VII, IN2P3-CNRS, Paris, France
[30] Institute of Physics, Academy of Sciences of the Czech Republic, Praha, Czech Republic[f,h]
[31] Nuclear Center, Charles University, Praha, Czech Republic[f,h]
[32] INFN Roma 1 and Dipartimento di Fisica, Università Roma 3, Roma, Italy
[33] Paul Scherrer Institut, Villigen, Switzerland
[34] Fachbereich Physik, Bergische Universität Gesamthochschule Wuppertal, Wuppertal, Germany[a]
[35] DESY, Institut für Hochenergiephysik, Zeuthen, Germany[a]
[36] Institut für Teilchenphysik, ETH, Zürich, Switzerland[i]
[37] Physik-Institut der Universität Zürich, Zürich, Switzerland[i]
[38] Institut für Physik, Humboldt-Universität, Berlin, Germany[a]
[39] Rechenzentrum, Bergische Universität Gesamthochschule Wuppertal, Wuppertal, Germany[a]
[40] Vistor from Yerevan Physics Institute, Armenia
[41] Foundation for Polish Science fellow
[42] Institut für Experimentelle Kernphysik, Universität Karlsruhe, Karlsruhe, Germany
[43] Department Fis. Ap. CINVESTAV, Mérida, Yucatán, México

Received: 10 March 1999 / Published online: 8 September 1999

Abstract. The electroproduction of J/ψ and $\psi(2S)$ mesons is studied in elastic, quasi-elastic and inclusive reactions for four momentum transfers $2 < Q^2 < 80$ GeV^2 and photon-proton centre of mass energies $25 < W < 180$ GeV. The data were taken with the H1 detector at the electron proton collider HERA in the years 1995 to 1997. The total virtual photon-proton cross section for elastic J/ψ production is measured as a function of Q^2 and W. The dependence of the production rates on the square of the momentum transfer from the proton (t) is extracted. Decay angular distributions are analysed and the ratio of the longitudinal and transverse cross sections is derived. The ratio of the cross sections for quasi-elastic $\psi(2S)$ and J/ψ meson production is measured as a function of Q^2. The results are discussed in terms of theoretical models based upon perturbative QCD. Differential cross sections for inclusive and inelastic production of J/ψ mesons are determined and predictions within two theoretical frameworks are compared with the data, the non-relativistic QCD factorization approach including colour octet and colour singlet contributions, and the model of Soft Colour Interactions.

1 Introduction

The high energy electron-proton collider HERA has renewed the interest in the study of light and heavy vector mesons produced in processes with quasi real and virtual photon exchange. Several production mechanisms valid in limited kinematic regions have been discussed in the literature for such processes and a unified picture is not available. The topics of the present paper are studies of elastic and inelastic production of J/ψ mesons and of quasi-elastic production of $\psi(2S)$ mesons for four momentum transfers $2 < Q^2 < 80$ GeV^2 and photon-proton centre of mass energies $25 < W < 180$ GeV.

Leptoproduction of J/ψ mesons has previously been studied in several fixed target experiments and at HERA in different kinematic regions [1–3]. In photoproduction, which corresponds to the limit $Q^2 \simeq 0$, and at low and medium Q^2 the production of J/ψ mesons, $e + p \to e + J/\psi + X$, is found to be dominated by processes where the hadronic system X is either a proton (elastic J/ψ production) or has a low mass M_X. These processes show characteristics of diffraction as observed in hadron–hadron interactions and in photoproduction of light vector mesons at lower energies. However, the experiments H1 and ZEUS have found that at HERA energies the dependence of the elastic J/ψ cross section on W in the photoproduction limit is steeper than measured in soft diffractive processes [4,5].

In recent years it has been demonstrated that elastic photo- and electroproduction of J/ψ mesons (Fig. 1a, c) can be calculated within perturbative QCD (pQCD) [6–9]. In these calculations the elastic cross section is related to the square of the gluon density in the proton and the fast rise of elastic J/ψ production with W reflects the increase of the gluon density in the proton at low values of Bjorken x [10]. According to these models elastic J/ψ meson production consequently offers a sensitive way to probe the gluon density. Further predictions of such models concern, for example, the fraction of longitudinally polarized J/ψ mesons, the dependences of the slope of the t distribution (t is the square of the momentum transfer from the proton) and of the ratio of $\psi(2S)$ to J/ψ meson production on kinematic variables. The latter ratio is also predicted in an approach based upon colour dipole phenomenology [11].

Inelastic J/ψ production, which can be described by the formation of $c\bar{c}$ states via boson gluon fusion (Fig. 1d, e), was previously studied in fixed target experiments [1, 12] and was analysed in the framework of the Colour Singlet Model [13]. At HERA inelastic J/ψ production has been analysed in photoproduction [4,14] and was successfully described by predictions of the Colour Singlet Model in next-to-leading order [15]. On the other hand, measurements of the production of J/ψ mesons in hadronic collisions [16] have shown that the Colour Singlet Model cannot account for the observed cross section. A good description of these data can, however, be achieved using a factorization approach in the framework of non-relativistic QCD (NRQCD) [17], where also colour octet states contribute. These colour octet processes are also expected to contribute in electroproduction. First analyses of HERA data showed that the color octet contribution in the photoproduction regime is less than expected [18]. In order to shed further light on the production process we present a fully inclusive analysis of J/ψ meson production in the range $0.2 < z \lesssim 1$, where z is the ratio of the energies of the J/ψ and the exchanged photon in the proton rest frame. In addition we extract inelastic cross sections in the same z range. The data are compared to calculations of lepton proton scattering in leading order performed in the NRQCD formalism [19] and to a phenomenological model incorporating Soft Colour Interactions [20] in the Monte Carlo generator AROMA [21].

The paper is organised as follows: after a discussion of different charmonium production models relevant for the present analysis and a description of the event selection, the total and differential cross sections for the elastic reaction $e + p \to e + J/\psi + p$ are presented with an extended kinematic reach compared to our previous measurement [2] and with statistics increased by an order of magnitude. We then report on the first measurement of $\psi(2S)$ production in deep inelastic scattering at HERA and extract the ratio of the $\psi(2S)$ to the J/ψ meson production cross section as a function of Q^2. Finally differential and total cross sections for inclusive and inelastic J/ψ production are presented.

2 Models and phenomenology

The experimental distinction between the various J/ψ production mechanisms discussed in the literature is not unambiguous and the following terminology will be adopted here. The process

$$e + p \to e + J/\psi + X$$

will be called "elastic" if X is a proton. Since the proton is in general not observed we use the term "quasi-elastic" for events in which only the tracks of the J/ψ decay leptons are present in the main detector. This data sample

[a] Supported by the Bundesministerium für Bildung, Wissenschaft, Forschung und Technologie, FRG, under contract numbers 7AC17P, 7AC47P, 7DO55P, 7HH17I, 7HH27P, 7HD17P, 7HD27P, 7KI17I, 6MP17I and 7WT87P
[b] Supported by the UK Particle Physics and Astronomy Research Council, and formerly by the UK Science and Engineering Research Council
[c] Supported by FNRS-FWO, IISN-IIKW
[d] Partially supported by the Polish State Committee for Scientific Research, grant no. 115/E-343/SPUB/P03/002/97 and grant no. 2P03B 055 13
[e] Supported in part by US DOE grant DE F603 91ER40674
[f] Supported by the Deutsche Forschungsgemeinschaft
[g] Supported by the Swedish Natural Science Research Council
[h] Supported by GA ČR grant no. 202/96/0214, GA AV ČR grant no. A1010821 and GA UK grant no. 177
[i] Supported by the Swiss National Science Foundation
[j] Supported by VEGA SR grant no. 2/5167/98
[k] Supported by Russian Foundation for Basic Research grant no. 96-02-00019

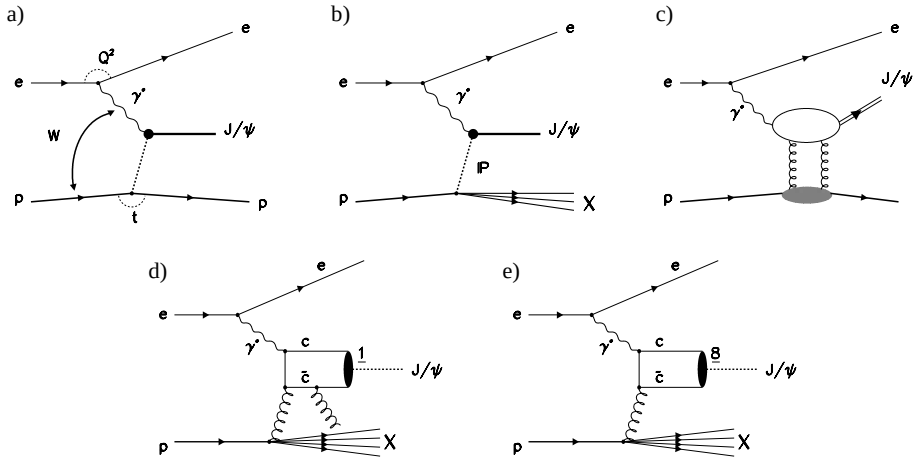

Fig. 1a–e. Charmonium production mechanisms: **a** elastic and **b** proton dissociative production via pomeron exchange; **c** elastic production via two-gluon exchange; **d** leading order diagram in the Colour Singlet Model (the $c\bar{c}$ pair is produced in a colour singlet state); **e** leading order Colour Octet Model (the $c\bar{c}$ pair is produced in a colour octet state)

comprises in addition to elastic events those in which the proton is diffractively excited into a system X dominantly of low mass, which subsequently dissociates (Fig. 1b). The decay or fragmentation products of this low mass system in general escape detection in the main detector. If a high mass system X is produced the emerging hadrons are usually detected and the process is called "inelastic". The term "inclusive" is used if only the presence of a J/ψ is demanded irrespective of the production and detection of other particles.

Elastic charmonium production. Elastic photoproduction of light vector mesons, ρ, ω and ϕ, is characterized by a weak dependence of the cross section on the photon-proton centre of mass energy W and by a diffractive peak, i.e. small scattering angle of the vector meson with respect to the incident photon direction. This behaviour is well described by vector meson dominance and Regge theory in terms of soft pomeron exchange (Fig. 1a). However, the cross section for elastic production of J/ψ mesons by quasi-real photons ($Q^2 \simeq 0$) at HERA is observed to rise steeply with W. Parameterizing the dependence as W^δ, δ is measured to be of order 1 for J/ψ mesons [4, 5], while light vector mesons show an energy dependence compatible with expectations from pomeron exchange in soft hadronic processes corresponding to $\delta \simeq 0.22 - 0.32$ (see [22]).

Modifications of the simple soft pomeron exchange model were subsequently proposed to describe the HERA data [23]. Alternatively an approach in the framework of pQCD [6–9] was pursued. In the models based on pQCD the interaction between the proton and the $c\bar{c}$ pair is mediated by a system of two gluons (Fig. 1c) or a gluon ladder and the fast increase of the cross section is related to the rise of the gluon density in the proton at small values of Bjorken x. Since the gluon density enters the cross section quadratically the sensitivity is large. In these calculations the scattering amplitude is obtained from the convolution of three contributions which are characterized by different time scales: the fluctuation of the (virtual) photon into a $c\bar{c}$ pair, the scattering of this hadronic system on the proton, and the formation of the final state vector meson.

In contrast to photoproduction where the charm quark mass offers the only hard scale (at low values of $|t|$), electroproduction of J/ψ mesons has an additional scale, Q^2, and at high Q^2 the predictions of perturbation theory are expected to become more reliable. Electroproduction of heavy vector mesons within pQCD was recently studied in great detail by Frankfurt et al. [9]. Important corrections were found concerning, for example, the choice of the scale at which the gluon density is probed, concerning the gluon distribution and the wave function for the vector meson and the importance of corrections due to Fermi motion of the quarks within the vector meson.

Inelastic charmonium production. In the Colour Singlet Model photo- or electroproduction of J/ψ mesons is assumed to proceed via boson gluon fusion into $c\bar{c}$ pairs which emerge in a colour singlet state due to the emission of an additional hard gluon (Fig. 1d). The failure of the Colour Singlet Model in describing hadroproduction of quarkonia at large transverse momenta led to new approaches for the description of J/ψ production which include contributions from $c\bar{c}$ pairs in colour octet states. The approach by Bodwin, Braaten and Lepage (BBL) [17] based on a factorization approach in NRQCD was suggested to describe the large hadroproduction rates for J/ψ and $\psi(2S)$ production at large p_t measured at the Tevatron [24].

When applied to J/ψ electroproduction [19], the cross section in the BBL formalism can be expressed as:

$$\sigma(e+p \to e+J/\psi+X) = \sum_n c_n(e+p \to e+c\bar{c}[n]+X)\langle \mathcal{O}_n^{J/\psi}\rangle, \qquad (1)$$

where $c\bar{c}[n]$ denotes an intermediate $c\bar{c}$ pair in a definite colour, spin and angular momentum state n. For each n, the cross section factorizes into a short distance part c_n calculable in a perturbative QCD expansion in the strong coupling parameter α_s and a long distance matrix element $\langle \mathcal{O}_n^{J/\psi}\rangle$ representing the probability for the $c\bar{c}[n]$ pair to evolve into a colour singlet J/ψ meson and additional soft gluons. The long distance matrix elements are not

calculable in perturbation theory and have to be determined experimentally or by lattice calculations, but they are thought to be universal.

The relative importance of the terms in (1) is determined by NRQCD scaling laws with respect to v, the typical relative velocity of the charm quarks in the $c\bar{c}$ system. In contrast to the Colour Singlet Model in which all c_n not corresponding to colour singlet $c\bar{c}$ states are neglected, the BBL formalism includes states where the $c\bar{c}$ system is in a colour octet state (Fig. 1e); therefore it is often called the "Colour Octet Model". However, colour octet contributions are suppressed by powers of v^2. Since v is small, $\langle v^2 \rangle \simeq 0.3$ [17], they only become important when the corresponding short distance coefficients c_n are large. In the limit $v \to 0$ the Colour Singlet Model is restored.

Soft colour interactions. The model of Soft Colour Interactions (SCI) was originally developed as an alternative to Regge phenomenology and pomeron exchange to describe diffractive scattering at HERA [25]. The model was successfully applied to quarkonia production at the Tevatron [20].

For electroproduction the model was implemented in the Monte Carlo program AROMA [21] which generates $c\bar{c}$ pairs via photon gluon fusion according to the leading order matrix elements approximating higher orders by parton showers. At a scale below the cut-off for pQCD additional interactions take place: quarks and gluons generated in the hard process interact non-perturbatively with the partons of the proton remnant; the latter are also allowed to interact with each other. In these soft colour interactions the momenta of the partons are not affected, only their colour states may change, which leads to a modification of the hadronic final state.

In such a model the conversion of a primary $c\bar{c}$ pair – which is in a colour octet state – into an observable colour singlet state such as J/ψ, χ_c, etc. may occur if the mass corresponds to the mass of the produced charmonium particle. The probability for this to happen is not constant as, for example, assumed in the Colour Evaporation Model [26] but depends on the final partonic state and, in the Lund string model, on the string configuration.

3 Detector, event selection, kinematics and simulations

The data presented here correspond to an integrated luminosity of 27.3 ± 0.4 pb^{-1}. They were collected in the years 1995 to 1997 using the H1 detector which is described in detail in [27]. HERA was operated with 27.5 GeV positrons and 820 GeV protons.

3.1 Detector and event selection

J/ψ mesons are detected via the decays $J/\psi \to \mu^+\mu^-$ and $J/\psi \to e^+e^-$ with branching fractions of $6.01\,(6.02) \pm 0.19\%$, respectively [28]. For $\psi(2S)$ mesons the decay $\psi(2S) \to J/\psi\,\pi^+\pi^-$ is used (branching ratio $30.2 \pm 1.9\%$ [28]) with the subsequent decay of the J/ψ into $\mu^+\mu^-$ or e^+e^-. The criteria for the data selection are summarised in Table 1; further details of the analysis can be found in [29].

In the Q^2 range studied here, the scattered positron is identified by its energy deposition in the backward electromagnetic calorimeter SpaCal [30] situated 152 cm backward from the nominal interaction point of the beams[1]. The SpaCal covers the polar angles $155^\circ < \theta < 178^\circ$ and has an energy resolution of $\sigma_E/E \simeq 7.5\%/\sqrt{E/\mathrm{GeV}} \oplus 2.5\%$. A minimal energy deposition of 14 GeV is required and cuts are applied to the cluster position and cluster shape in order to ensure high trigger efficiency and a good quality positron measurement. To keep acceptance corrections small, the Q^2 range is limited to $2 < Q^2 < 80$ GeV^2. A drift chamber (BDC) in front of the SpaCal is used to reconstruct the polar angle θ_e of the scattered positron in combination with the interaction vertex.

The decay leptons of the J/ψ meson are detected in the central tracking detector (CTD), consisting mainly of two coaxial cylindrical drift chambers, which have a length of 2.2 m and outer radii of 0.45 m and 0.84 m. The charged particle momentum component transverse to the beam direction is measured in these chambers by the track curvature in the 1.15 T magnetic field generated by the superconducting solenoid, with the field lines directed along the beam axis. Two polygonal drift chambers with wires perpendicular to the beam direction, which are located respectively at the inner radii of the two chambers, are used to improve the measurement of the particle polar angle. The tracking system is complemented in the forward direction by a set of drift chambers with wires perpendicular to the beam direction which allow particle detection for polar angles $\theta \gtrsim 7^\circ$. Multiwire proportional chambers serve for triggering purposes.

In the present analyses, two oppositely charged tracks with transverse momenta p_t larger than 0.1 GeV are required to be reconstructed in the CTD with polar angles in the range $20^\circ < \theta < 160^\circ$ where the detection efficiency is high. For each event, the vertex position in z is determined using tracks reconstructed in the CTD. To suppress background from interactions of the beam with residual gas in the beam pipe, the vertex must be reconstructed within 40 cm from the nominal interaction point corresponding to 3.5 times the width of the vertex distribution.

For the study of elastic J/ψ production to suppress background from inelastic reactions no track, except a possible track from the scattered positron, is allowed to be present in addition to the tracks from the two decay leptons. In the $\psi(2S)$ analysis exactly two tracks, assumed to be pions, with transverse momenta above 0.12 GeV and opposite charge are required in addition to the two decay leptons (an additional track from the scattered positron

[1] H1 uses a right handed coordinate system, the forward ($+z$) direction, with respect to which polar angles are measured, is defined as that of the incident proton beam, the backward direction ($-z$) is that of the positron beam

Table 1. Summary of selection criteria for the different data sets

I. Quasi-Elastic J/ψ CTD-CTD $40 < W < 160$ GeV, $2 < Q^2 < 80$ GeV^2	
Tracks	Reconstructed event vertex with $\lvert z_{vtx} - z_{nom}\rvert < 40$ cm Exactly 2 tracks in CTD[a] Opposite charges, $20^\circ < \theta < 160^\circ$, $p_t > 0.1$ GeV
Decay leptons	≥ 1 μ identified in LAr Cal. (LAr) or Central Muon Detector (CMD) *or* 2 e identified in LAr Calorimeter
Other	Forward untagged: $E^{10^\circ}_{LAr} < 1$ GeV and $N_{PRT} = 0$ and $N_{FMD} < 2$ Forward tagged: $E^{10^\circ}_{LAr} > 1$ GeV or $N_{PRT} > 0$ or $N_{FMD} \geq 2$
II. Quasi-Elastic J/ψ FMD-CTD (FMD-FMD) $25 < W < 40$ GeV, $2 < Q^2 < 6$ GeV^2	
Decay μ	1 μ in FMD and 1 μ in CTD+LAr/CMD as in I. *or* 2 μ in FMD Opposite charges
Other	No tracks except those associated with the decay muons [a]
III. Quasi-elastic $\psi(2S)$ $40 < W < 180$ GeV, $1 < Q^2 < 80$ GeV^2	
Decay particles	Reconstructed event vertex with $\lvert z_{vtx} - z_{nom}\rvert < 40$ cm Exactly 4 tracks in CTD[a] 2 μ identified in LAr or CMD *or* 2 e identified in LAr Opposite charges of the two leptons and of the two additional tracks (pions) $20^\circ < \theta < 160^\circ$, $p_t > 800$ MeV (leptons), $p_t > 120$ MeV (π^+, π^-)
IV. Inclusive and Inelastic J/ψ $40 < W < 180$ GeV, $2 < Q^2 < 80$ GeV^2	
Tracks	Reconstructed event vertex with $\lvert z_{vtx} - z_{nom}\rvert < 40$ cm
Decay leptons	2 μ identified in LAr or CMD *or* 2 e identified in LAr Opposite charges, $20^\circ < \theta < 160^\circ$ and $p_t > 800$ MeV
Inelastic selection	$E_{fwd} > 5$ GeV
General	
Scattered e^+	$E_e > 14$ GeV identified in SpaCal
Final state	$\sum(E - p_z) > 45$ GeV

[a] Any additional track associated with the scattered e^+ is not considered here

is allowed). In the study of inclusive J/ψ production no requirement on the track multiplicity is imposed. An inelastic data set is defined by the additional requirement of an energy deposition of $E_{fwd} > 5$ GeV in the forward region of the liquid argon (LAr) calorimeter at polar angles $\theta < 20^\circ$.

The J/ψ decay leptons are identified by the LAr calorimeter surrounding the tracking detectors and situated inside the solenoid. The LAr calorimeter is segmented into electromagnetic and hadronic sections and covers the polar angular range $4^\circ < \theta < 154^\circ$ with full azimuthal coverage. Muons which are identified as minimum ionizing particles in the LAr calorimeter can in addition be identified by track segments reconstructed in the instrumented iron return yoke (central muon detector CMD, $4^\circ < \theta < 171^\circ$) and in the forward muon detector (FMD, $3^\circ < \theta < 17^\circ$). The FMD provides track segments in front of and behind a toroidal magnet with a field of $B = 1.5 - 1.75$ T, thus allowing a determination of the muon momentum with a precision of about 25%.

The lepton selection criteria vary for the different data sets, depending on the amount of background. For the quasi-elastic event selection, the identification of *one muon* or *two electrons* is required. For the $\psi(2S)$ and the inclusive data sets two identified leptons with transverse momenta $p_t > 0.8$ GeV are required.

A dedicated analysis has been carried out to extend the analysis of elastic J/ψ production towards small W ($25 < W < 40$ GeV) using the FMD ("Low W analysis"). Two data sets are selected. The events of the first set which are required to have one decay muon in the FMD and the other one in the CTD (FMD-CTD) are

used for a cross section determination. In the second data set both muons are measured in the FMD (FMD-FMD) with an additional loose vertex requirement to suppress muons originating from the proton beam halo. The latter set ($20 < W < 35$ GeV) serves as a control sample for the FMD efficiency which was also determined from a larger photoproduction J/ψ sample. Due to statistical limitations, the low W analysis is restricted to the low Q^2 ($2 < Q^2 < 6$ GeV^2) region.

The triggers in all analyses require a total energy deposition in the SpaCal above a threshold of $6-12$ GeV. The value of the threshold depends on the topology of the energy deposition and on the presence of additional requirements, such as signals from the central drift chambers and/or the multiwire proportional chambers.

In order to minimise the effects of QED radiation in the initial state, the difference between the total energy and the total longitudinal momentum $\sum(E-p_z)$ reconstructed in the event is required to be larger than 45 GeV. If no particle, in particular a radiated photon, has escaped detection in the backward direction, the value of $\sum(E-p_z)$ is twice the incident positron energy, i.e. 55 GeV.

Forward region. After requiring exactly two tracks corresponding to the J/ψ decay leptons the event sample includes two main contributions: elastic events and events with proton dissociation. It is possible to identify most of the proton dissociation events with the components of the detector in the forward region, namely the forward part of the LAr calorimeter, $4^\circ \leq \theta \leq 10^\circ$, the forward muon detector FMD and the proton remnant tagger (PRT, an array of scintillators 24 m downstream of the interaction point, $0.06^\circ \leq \theta \leq 0.17^\circ$). When particles from the diffractively excited system interact with the material in the beam pipe or with the collimators, the interaction products can be detected in these forward detectors. Events are "tagged" as candidates for proton dissociation by the presence of a cluster with energy E_{LAr} larger than 1 GeV at an angle $\theta < 10^\circ$ in the LAr calorimeter, or by at least 2 pairs of hits in the first three layers of the FMD ($N_{FMD} \geq 2$), or by at least one hit in the proton remnant tagger ($N_{PRT} > 0$). The forward detectors are sensitive to $M_X \gtrsim 1.6$ GeV.

3.2 Kinematics

The kinematics for charmonium production is described with the standard variables used for deep inelastic interactions, namely the square of the ep centre of mass energy, $s = (p+k)^2$, $Q^2 = -q^2$ and $W = (p+q)^2$, where k, p and q are the four-momenta of the incident positron and proton and of the virtual photon. In addition, the scaled energy transfer $y = p \cdot q / p \cdot k$ (energy fraction transferred from the positron to the hadronic final state in the proton rest frame) and the Bjorken variable $x = Q^2/2p \cdot q$ are used. Neglecting the positron and proton masses the following relations hold: $Q^2 = xys$ and $W^2 = ys - Q^2$.

In the case of elastic J/ψ and quasi-elastic $\psi(2S)$ production the kinematic variables are reconstructed with the "double angle" method [31], where Q^2 and y are computed using the polar angles θ and γ of the positron and of the vector meson in the HERA laboratory frame of reference, which are well measured:

$$Q^2 = 4E_0^2 \frac{\sin\gamma(1+\cos\theta)}{\sin\gamma + \sin\theta - \sin(\gamma+\theta)}, \tag{2}$$

$$y = \frac{\sin\theta(1-\cos\gamma)}{\sin\gamma + \sin\theta - \sin(\gamma+\theta)}; \tag{3}$$

E_0 denotes the energy of the incident positron. The momentum components of the J/ψ and the $\psi(2S)$ mesons are obtained from their measured decay products.

Since the fractional energy loss of the proton is negligible, the absolute value of the four momentum transfer t is given to a good approximation by the following relation[2]:

$$|t| \simeq (\vec{p}_{tp})^2 = (\vec{p}_{te} + \vec{p}_{tv})^2, \tag{4}$$

where $\vec{p}_{tp}$, $\vec{p}_{te}$ and $\vec{p}_{tv}$ are, respectively, the momentum components transverse to the beam direction of the final state proton, positron[3] and vector meson. The resolution obtained from the Monte Carlo simulation for the reconstruction of W ranges from 4 to 9% depending on Q^2. For Q^2 it is about 2%, and for t on average 0.10 GeV^2.

The variable $\sum(E-p_z)$ is computed as:

$$\sum(E-p_z) = (E_e + E_v) - (p_{ze} + p_{zv}), \tag{5}$$

E_e and E_v being the measured energies of the scattered positron and of the vector meson, and p_{ze} and p_{zv} their momentum components parallel to the beam direction.

For inclusive J/ψ production, the "$e\Sigma$" method [32] is used to reconstruct the event kinematics, which combines the measurement of both the scattered positron and the full hadronic final state to obtain good resolution over the entire kinematic region. The variable Q^2 is reconstructed from the scattered positron. For the calculation of y and the elasticity $z = (p_\psi \cdot p)/(q \cdot p)$, where p_ψ denotes the J/ψ four-momentum, the observed final state is used in addition. Thus

$$y = \frac{\sum_{had}(E-p_z)}{\sum(E-p_z)} \quad \text{and} \quad z = \frac{(E-p_z)_\psi}{\sum_{had}(E-p_z)}, \tag{6}$$

where the sums run over all particles observed in the final state, but excluding the scattered positron in those indicated by "had". For the calculation of the sums in equation (6) a combination of tracks reconstructed in the CTD and cells in the LAr and SpaCal calorimeters is used. The resolution is good ($2-5$%) for the variables Q^2, $p^2_{t,\psi}$ and y^*, the rapidity of the J/ψ in the $\gamma^* p$ centre of mass frame. For z (W) the resolution is 2% (3%) for $z > 0.9$ and on average 17% (9%) for $z < 0.9$.

[2] The lowest $|t|$ value kinematically allowed, $t_{min} \simeq (Q^2 + m_V^2)^2\ m_p^2\ /y^2 s^2$, is negligibly small

[3] The momentum of the scattered positron is here computed from Q^2 and y, which provides better precision than the direct SpaCal energy measurement

3.3 Monte Carlo simulations

To take account of detector acceptance and efficiencies, smearing effects, losses due to the selection criteria, and remaining backgrounds, corrections are applied to the data using Monte Carlo simulations. The H1 detector response is simulated in detail, and the simulated events are passed through the same reconstruction and analysis chain as the data.

The correct description of the data by the simulation has been checked extensively by independent measurements and was adjusted where necessary. In particular, the trigger efficiencies have been determined using independent data sets, the efficiency of the central drift chambers has been measured using cosmic ray muons, and the lepton identification probabilities have been determined using control samples in which the J/ψ is reconstructed identifying only one or no lepton. Remaining differences between data and simulation are used to estimate systematic uncertainties.

Typical efficiencies are: lepton identification $\sim 80\%$ per lepton, track reconstruction $\sim 96\%$ per track, and identification of the scattered positron 99%. The total trigger efficiency is determined to be 97% on average.

The following event generators are used:

- The **DIFFVM** program [33] is based on the Vector Meson Dominance Model and permits variation of the Q^2, W and t dependences, as well as a variation of the value of $R = \sigma_L/\sigma_T$. In addition to the elastic process, vector meson production with proton dissociation is simulated where the dependence of the cross section on the mass M_X of the dissociated hadronic state X is parameterized as $1/M_X^{2.16}$. High mass states are assumed to decay according to the Lund string model [34]. In the resonance domain, the mass distribution is modelled using measurements from target dissociation on deuterium [35], and resonance decays are described using their known branching ratios.
- **EPJPSI** [36] implements inelastic J/ψ production according to the Colour Singlet Model taking into account relativistic corrections and parton showers.
- The **LPAIR** generator [37] simulates QED electron- and muon-pair production, $\gamma\gamma \to e^+e^-$ and $\gamma\gamma \to \mu^+\mu^-$, where the photons originate from the positron and proton respectively. Elastic and inelastic processes are simulated.

Radiative corrections. The measured cross sections are given in the QED Born approximation for electron interactions. The effects of higher order processes – mainly initial state radiation – are estimated using the HECTOR program [38].

Radiative corrections for the double angle reconstruction (elastic J/ψ and quasi-elastic $\psi(2S)$ production) are about $2-3\%$, and are weakly dependent on Q^2 and W. A systematic uncertainty of 3% is obtained by variation of the Q^2 and W dependences of the $\gamma^* p$ cross section within the uncertainties of the measurement. For the reconstruction of kinematics according to the $e\Sigma$ method (used in the inclusive J/ψ analysis) the radiative corrections amount to $6-8\%$, and again are only weakly dependent on Q^2 and W.

Table 2. Slope parameters b of the elastic J/ψ meson t distribution for different Q^2 and W domains

$40 < W < 160$ GeV	
$2 < Q^2 < 8$ GeV^2	$8 < Q^2 < 80$ GeV^2
$b = 4.4 \pm 0.4 \pm 0.4$ GeV^{-2}	$b = 2.5 \pm 0.6 \pm 0.6$ GeV^{-2}
$2 < Q^2 < 80$ GeV^2	
$40 < W < 100$ GeV	$100 < W < 160$ GeV
$b = 4.0 \pm 0.4 \pm 0.4$ GeV^{-2}	$b = 4.1 \pm 0.5 \pm 0.5$ GeV^{-2}

Table 3. Integrated cross sections for $40 < W < 180$ GeV, $Q^2 < 80$ GeV^2 and $z > 0.2$ in two kinematic regions, $Q^2 > 2.0$ GeV^2 and Q^2 and $p^2_{t,\psi} > 4.0$ GeV^2. Results are given for the inclusive selection and for two inelastic selections, $M_X > 10$ GeV and $z < 0.9$

Data set	$\sigma(ep \to e\, J/\psi\, X)$ [nb]	
	$Q^2 > 2.0$ GeV^2	$Q^2, p^2_{t,\psi} > 4.0$ GeV^2
Inclusive	$1.30 \pm 0.06 \pm 0.24$	$0.50 \pm 0.04 \pm 0.09$
$M_X > 10$ GeV	$0.51 \pm 0.04 \pm 0.09$	$0.17 \pm 0.02 \pm 0.03$
$z < 0.9$	$0.46 \pm 0.04 \pm 0.09$	$0.13 \pm 0.02 \pm 0.02$

4 Elastic J/ψ production

The distributions of the invariant mass m_{ll} for the selected events in the J/ψ region with two tracks in the central region are presented in Fig. 2a and b, for the $\mu^+\mu^-$ and the e^+e^- decay channels, respectively (data set CTD-CTD, I. in Table 1) . A clear signal is observed at 3.090 ± 0.005 GeV, compatible with the nominal J/ψ mass of 3.097 GeV [28]. The peak width is compatible with the expectation obtained from the detector simulation. The mass spectra for the events in the low W analysis where one or both muons are reconstructed in the forward muon detector (FMD) are shown in Fig. 3a and b (data sets FMD-FMD and FMD-CTD, II. in Table 1).

For the events with two tracks in the central detector the J/ψ signal region is defined by the condition $|m_{ll} - m_\psi| < 250$ MeV, where m_ψ is the nominal J/ψ mass. The non-resonant background under the J/ψ peak is determined by fitting the sidebands using an exponential distribution and is found to be $12 \pm 3\%$ on average. The error includes the uncertainties of the resonance parameterization and of the background shape where the latter was estimated using a power law as alternative. The non-resonant background is mainly due to dilepton production by two photons as simulated by the Monte Carlo generator LPAIR, but there is also a contribution from hadrons misidentified as leptons. Some distributions for events in the signal region are shown in Fig. 4 as well as the predictions from a diffractive simulation, DIFFVM. The distributions for the scattered positron and for the reconstructed J/ψ meson are reasonably well described by the

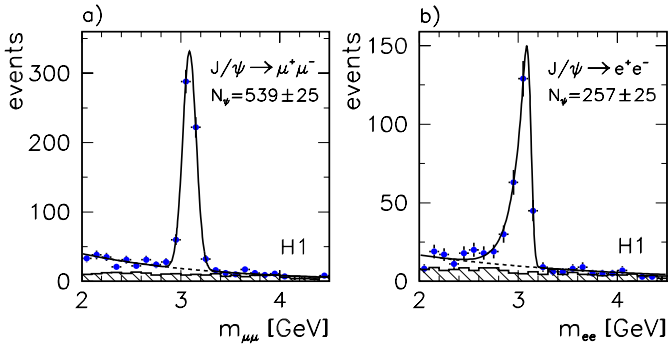

Fig. 2a,b. Mass spectra for events of the quasi-elastic J/ψ selection: **a** $\mu^+\mu^-$ pairs, **b** e^+e^- pairs. Both particles are detected in the central region. The full lines are the results of a fit using a Gaussian distribution for the signal region (convoluted with an exponential tail to account for energy loss in the case of di-electron decays) and an exponential distribution for the non-resonant background. The mass spectra from two photon processes (LPAIR simulation) are shown as hatched histograms. N_ψ is the number of J/ψ events obtained from the fit

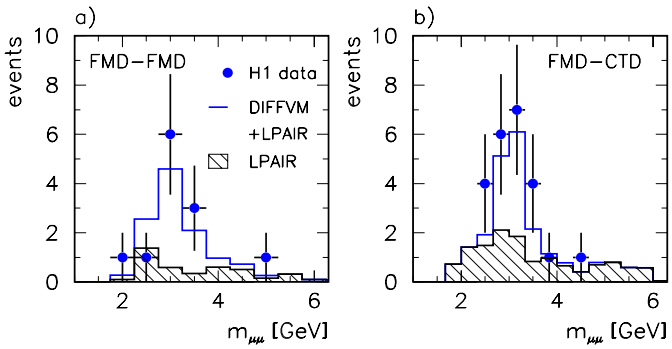

Fig. 3a,b. Mass spectra for events of the J/ψ selection in the low W analysis: **a** $\mu^+\mu^-$ pairs for the FMD-FMD sample and **b** for the FMD-CTD sample. The open histogram represents the prediction of a Monte Carlo simulation including diffractively produced J/ψ mesons (DIFFVM) and muon pairs from two photon processes (LPAIR) which are also shown separately as hatched histograms

simulation. Remaining differences between data and simulation were checked to have a small impact on the results and are accounted for by the systematic uncertainty.

The distribution of the quasi-elastic J/ψ events from the three data sets (CTD-CTD, FMD-CTD and FMD-FMD) in the kinematic plane x versus Q^2 is displayed in Fig. 5 before applying Q^2 and W cuts.

4.1 Cross sections as functions of W and Q^2

In order to measure the elastic cross section, the quasi-elastic data sample is divided into two non overlapping classes, *forward untagged* and *forward tagged* (see Table 1, I.), which are enriched in elastic and proton dissociation processes, respectively. The data are binned in Q^2 and W and the non-resonant background is determined and

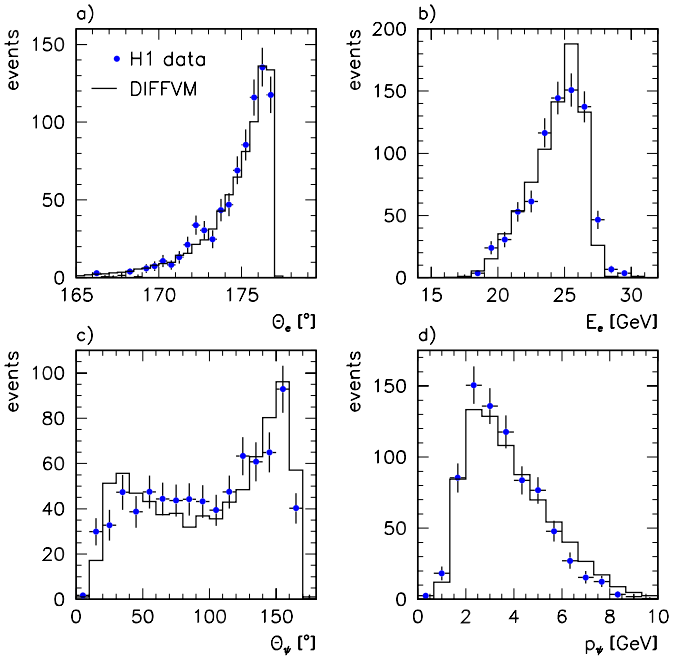

Fig. 4a–d. Control distributions for the quasi-elastic J/ψ selection (data set I. in Table 1). **a** Polar angle and **b** energy of the scattered positron, **c** polar angle and **d** momentum of the reconstructed J/ψ candidates. The error bars on the data points are statistical only. Results of a diffractive Monte Carlo simulation (DIFFVM) normalised to the data are shown as histograms

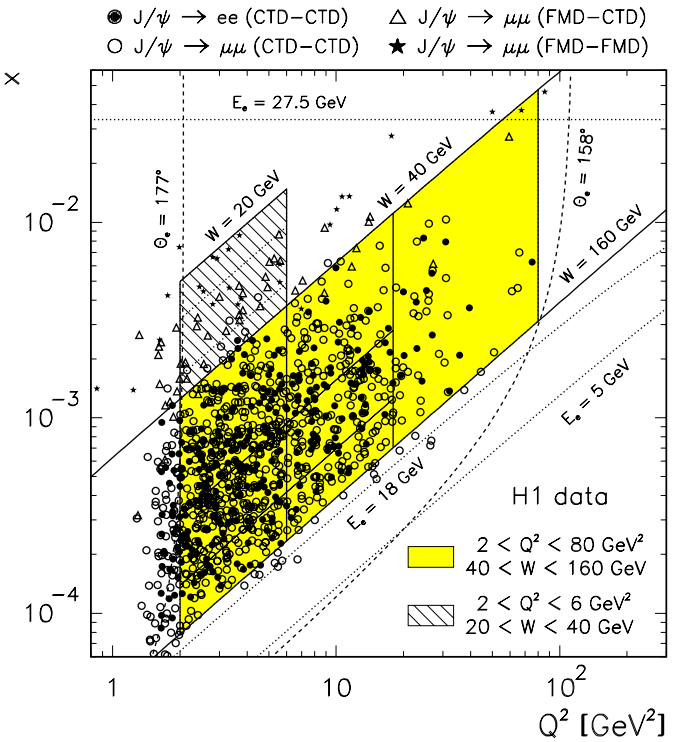

Fig. 5. Distribution of quasi-elastic J/ψ candidates in the kinematic (x, Q^2) plane (data sets I. and II. in Table 1), before applying Q^2 and W cuts. Lines of constant W, energy E_e and polar angle θ_e of the scattered positron are shown and the different analysis regions are indicated

subtracted for each bin. The "true" numbers of elastic and proton dissociative events N_{el} and N_{pd} are extracted by unfolding them from the number of events with and without a tag of the forward detectors (see Sect. 3.1). The efficiencies for tagging and for non-tagging of elastic and proton dissociative events are determined by studying the response of the forward detectors and are incorporated in the detector simulation. The tagging efficiency for proton dissociative events with $M_X \gtrsim 1.6$ GeV is found to be 92% on average[4]. Note that in this procedure no assumption is made for the absolute or relative cross sections of the two processes.

A small correction ($\simeq 3\%$) due to the presence of spurious hits in the FMD which are not described by the Monte Carlo simulation is applied. Further corrections account for the contamination from decays of the $\psi(2S)$ meson into a J/ψ and undetected neutral particles (based on the results of section 5) and for initial state radiation (section 3.3). Using the integrated luminosity and the sum of the branching fractions for the J/ψ meson to decay into $\mu^+\mu^-$ or e^+e^-, an integrated ep cross section is calculated for each Q^2 and W bin.

In the Born approximation, the electroproduction cross section is related to the $\gamma^* p$ cross section by

$$\frac{d^2\sigma(ep \to eJ/\psi\, p)}{dy\; dQ^2} = \Gamma\sigma(\gamma^* p \to J/\psi\, p) = \Gamma\sigma_T(\gamma^* p \to J/\psi\, p)(1+\varepsilon R), \quad (7)$$

where $R = \sigma_L/\sigma_T$, σ_T and σ_L are the transverse and longitudinal $\gamma^* p$ cross sections. Γ is the flux of transverse virtual photons [39] and ε is the flux ratio of longitudinally to transversely polarized photons, given by

$$\Gamma = \frac{\alpha_{em}}{2\pi\; y\, Q^2} \cdot (1+(1-y)^2); \qquad \varepsilon = \frac{1-y}{1-y+y^2/2}. \quad (8)$$

Virtual photon-proton cross sections are computed using equation (7) after integrating over the Q^2 and W bins used in the analysis. The difference between $\sigma(\gamma^* p \to J/\psi p) = \sigma_T + \varepsilon\sigma_L$ and $\sigma_{tot}(\gamma^* p \to J/\psi p) = \sigma_T + \sigma_L$ is negligible here since $\langle\varepsilon\rangle = 0.99$.

For the analysis in which both tracks are detected in the central detector the systematic uncertainties of the cross sections are estimated to be 17% in total, and are only slightly dependent on the kinematics. They consist of uncertainties due to detector efficiencies and resolution (10%), uncertainties in the estimation of background (11%, dominated by proton dissociation and $\psi(2S)$ decays), radiative corrections and bin centre determination (4%), the J/ψ decay branching ratio, and luminosity determination (4%). Part of the systematic error (9%) affects only the overall normalization. The uncertainty arising from the proton dissociation background is estimated by varying the cuts to select proton dissociation events, by changing the M_X dependence assumed in the Monte Carlo simulation, and by changing the model used for the fragmentation of the system X. The uncertainty due to the subtraction of non-resonant background is determined by varying the assumed shape of the background and using alternative methods for its determination, such as sideband subtraction.

For the low W analysis (one muon in the FMD) a different procedure to extract the cross section was adopted due to limited statistics. Since the contribution of hadrons misidentified as muons is negligible here, the non-resonant background is subtracted using the LPAIR Monte Carlo simulation. Alternatively it is estimated from the sidebands of the mass spectrum. The proton dissociation background is subtracted assuming the same fraction as determined in the CTD-CTD analysis; this assumption was verified by comparing the response of the forward detectors, taking into account the effect of the forward going muon. The efficiency of the FMD is determined using a sample of J/ψ photoproduction events and is cross checked by the control sample with both muons in the FMD. On average, the FMD efficiency is found to be $\sim 81\%$. The total systematic uncertainty of the cross section in the low W analysis is 25%, dominated by the uncertainties in the subtraction of non-resonant and proton dissociation backgrounds and by the uncertainty of the FMD efficiency.

The $\gamma^* p$ cross sections are shown in Fig. 6 and are given in Table 4 as functions of W in three bins of Q^2 ($2 < Q^2 < 6$ GeV^2, $6 < Q^2 < 18$ GeV^2 and $18 < Q^2 < 80$ GeV^2). Also shown are measurements of the ZEUS collaboration[5] at similar values of Q^2. The cross sections of the present analysis are quoted at values of W and Q^2 after applying bin centre corrections using the measured W and Q^2 dependences. The W dependence, which in pQCD based models is related to the x dependence of the gluon density in the proton, is found to be similar to that obtained in the photoproduction limit at HERA (also shown in Fig. 6). When parameterized in the form W^δ, fits to H1 and ZEUS photoproduction data yield $\delta = 0.77 \pm 0.18$, while the H1 data for $Q^2 > 0$ yield $\delta = 0.84 \pm 0.20$ at $Q^2 = 3.5$ GeV^2 and $\delta = 1.3 \pm 0.4$ at $Q^2 = 10.1$ GeV^2, where the errors include statistical and systematic uncertainties. The fits are shown in Fig. 6.

In Fig. 6 also predictions of the model by Frankfurt et al. [9] are included. Gluon densities from GRV(HO) [40] and MRSR2 [41] are used at an effective scale depending on Q^2 and on the separation of the quarks within the J/ψ. The prediction using MRSR2 describes the slope of the data well while the calculation using GRV(HO) is too steep at low values of Q^2. At small Q^2, $Q^2 \lesssim 10$ GeV^2, the absolute magnitudes of the predictions are very sensitive to the input value for the charm quark mass ($m_c = 1.4$ GeV was chosen here), as is indicated by the arrows in Fig. 6: For $Q^2 = 0$ and $W = 200$ GeV, for example, a

[4] The contribution of small masses $M_X \lesssim 1.6$ GeV, for which the tagging efficiency is below 50%, amounts to about 15% of the proton dissociation cross section according to the Monte Carlo simulation

[5] In the present paper, we do not use fixed target data for comparison because experimental conditions and methods are different and lead to uncertainties in the comparison: for example most experiments used heavy nuclei as targets and define elastic processes differently

Table 4. Cross sections for the elastic process $\gamma^* p \to J/\psi\, p$ in bins of W for three Q^2 regions: $2 < Q^2 < 6$ GeV^2, $6 < Q^2 < 18$ GeV^2 and $18 < Q^2 < 80$ GeV^2

$\langle Q^2 \rangle$ [GeV^2]	W interval [GeV]			$\langle W \rangle$ [GeV]	$\sigma(\gamma^* p \to J/\psi p)$ [nb]		
3.5	25	–	40	32.0	11.7	± 3.2 (stat.)	± 2.9 (syst.)
	40	–	60	49.3	22.5	± 4.0	± 3.6
	60	–	80	69.5	26.3	± 3.9	± 4.2
	80	–	100	89.6	33.1	± 5.1	± 5.2
	100	–	120	109.6	30.7	± 5.8	± 4.8
	120	–	160	138.6	54.9	± 8.9	± 8.8
10.1	40	–	80	57.5	5.4	± 1.3	± 0.9
	80	–	120	98.4	10.3	± 2.2	± 1.7
	120	–	160	138.6	17.8	± 4.2	± 3.1
33.6	40	–	160	84.4	1.34	± 0.37	± 0.24

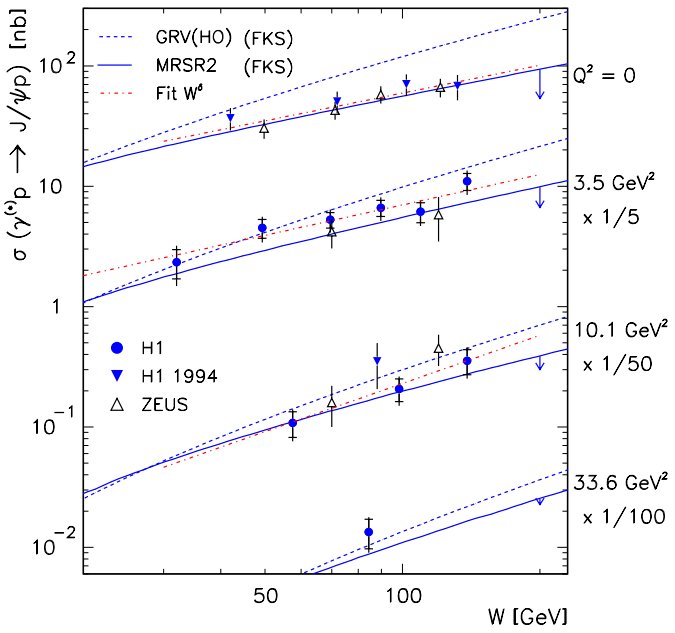

Fig. 6. Cross sections for elastic J/ψ production as a function of W at different values of Q^2, measured at HERA in this and other analyses [2–5]. Data for $Q^2 > 0$ have been scaled by factors 5, 50 and 100 as indicated. The inner error bars on the points from this analysis indicate the statistical errors, while the outer bars show the statistical and systematic uncertainties added in quadrature. The dash-dotted lines are the results of fits of the form W^δ to the data for each Q^2. For $Q^2 > 0$ the fits are for H1 data only. The full and dashed lines are results of calculations from Frankfurt et al. [9] using different parameterizations of the proton gluon densities. The small arrows at $W = 200$ GeV indicate the sensitivity of this prediction to a change of the charm quark mass from 1.4 GeV to 1.5 GeV

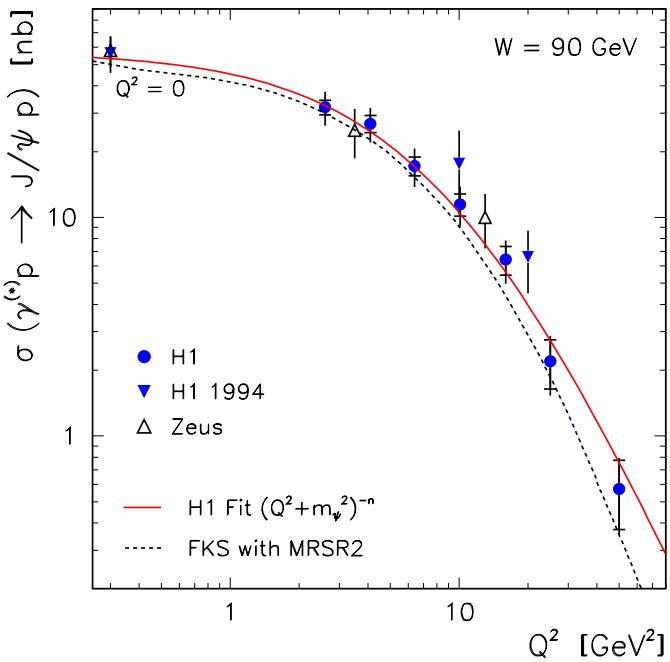

Fig. 7. The cross section for elastic J/ψ production at $W = 90$ GeV as a function of Q^2. The inner error bars on the points from this analysis indicate the statistical errors, while the outer bars show the statistical and systematic uncertainties added in quadrature. Also shown are previous measurements in photoproduction (indicated by $Q^2 = 0$) [4,5] and deep inelastic scattering [2,3]. The full line is a fit of the form $(Q^2 + m_\psi^2)^{-n}$, yielding the result $n = 2.38 \pm 0.11$. The dashed line is the prediction of Frankfurt et al. [9] using the MRSR2 [41] gluon density

change from $m_c = 1.4$ GeV to $m_c = 1.5$ GeV reduces the prediction by more than 40%.

The Q^2 dependence of the cross section for W=90 GeV ($40 < W < 160$ GeV) is shown in Fig. 7 and given in Table 5. It is well described by a fit $\propto (Q^2 + m_\psi^2)^{-n}$ with $n = 2.38 \pm 0.11$. In order to study a possible change in the observed Q^2 dependence, which may be an indication for the importance of non-perturbative effects, the fits are repeated in two Q^2 regions leading to $n = 2.12 \pm 0.20$ for $Q^2 < 12$ GeV^2 and $n = 2.97 \pm 0.51$ for $Q^2 > 12$ GeV^2. The errors contain statistical and systematic uncertainties. In Fig. 7 the model of Frankfurt et al. with the MRSR2 gluon

Table 5. Q^2 dependence of the elastic cross section $\sigma(\gamma^* p \to J/\psi\, p)$

Q^2 interval [GeV^2]	$\langle Q^2 \rangle$ [GeV^2]	$\sigma(\gamma^* p \to J/\psi p)$ ($W = 90$ GeV) [nb]	
2.0 – 3.2	2.6	31.9 ± 2.5 (stat.)	± 5.1 (syst.)
3.2 – 5.0	4.1	26.8 ± 2.4	± 4.2
5.0 – 8.0	6.4	17.2 ± 1.7	± 3.0
8.0 – 12.7	10.1	11.5 ± 1.3	± 2.0
12.7 – 20.1	16.0	6.4 ± 1.0	± 1.1
20.1 – 31.8	25.0	2.20 ± 0.55	± 0.38
31.8 – 80.0	50.0	0.57 ± 0.20	± 0.10

distribution which was seen to give a good description of the W dependence (Fig. 6) is also compared to the data. The Q^2 dependence is reasonably well described by the prediction.

4.2 t distribution and elastic slope parameter

The elastic slope parameter b is determined assuming that the t dependence of the elastic J/ψ cross section can be parameterized by a single exponential distribution e^{bt}. Three contributions are fitted to the forward untagged J/ψ sample, corrected for acceptance, losses and smearing effects. These are:

- One exponential distribution e^{bt} with a slope b as free parameter describing elastic J/ψ production.
- The non-resonant background is described by the sum of two exponential distributions contributing in total 12%. The t-slopes of the non-resonant background are determined using the sidebands of the J/ψ mass distribution. The background fraction depends strongly on t. For the estimation of the systematic uncertainty, the total amount is varied within the range $5 - 16\%$.
- The proton dissociation background is described by one exponential with a slope parameter 1.4 GeV^{-2}. This is compatible with studies of the forward tagged data set taking into account non-resonant background. The total contribution is fixed to 13% and is varied between 5% and 28% to estimate the systematic error, while the slope was varied between 0.8 GeV^{-2} and 2.0 GeV^{-2}.

No correction for background from $\psi(2S)$ decays is applied since the total contribution is small at low Q^2. The result of the fit which is carried out up to $|t| = 1.2$ GeV^2 is shown in Fig. 8 ($\chi^2/NDF = 1.6/4$). The elastic slope parameter is

$$b = 4.1 \pm 0.3\ (\text{stat.}) \pm 0.4\ (\text{syst.})\ \text{GeV}^{-2} \qquad (9)$$

for mean values $\langle W \rangle = 96$ GeV and $\langle Q^2 \rangle = 8$ GeV^2. The systematic uncertainty was estimated by varying the fit range by ±0.4 GeV^2 and by varying the background contributions and the corresponding slopes within the ranges given above.

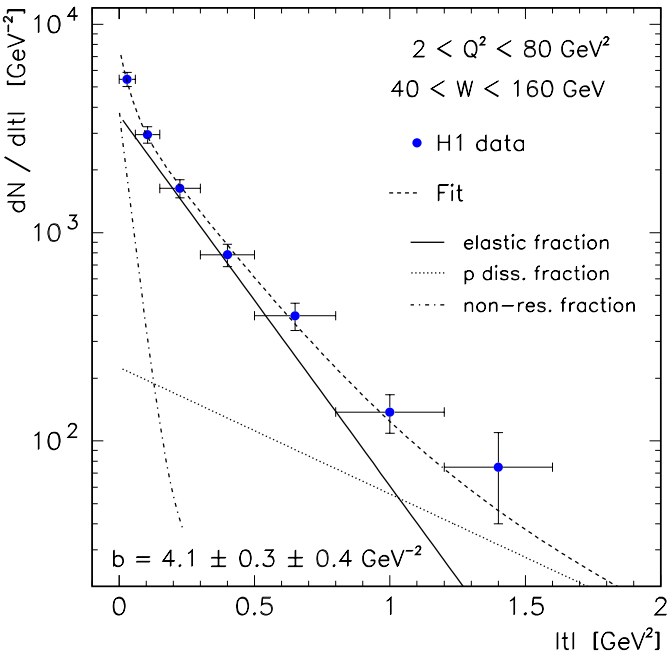

Fig. 8. $|t|$ distribution for the forward untagged J/ψ sample, corrected for acceptance, losses and smearing effects. The dashed line is the result of a fit taking the background contributions into account as described in the text. The full line corresponds to the elastic contribution assuming an exponential distribution. The contributions from proton dissociation and non-resonant background are shown separately. The error bars on the data points are statistical only

This result for b is compatible with the values obtained by H1 [4] and ZEUS [5] for elastic J/ψ photoproduction at similar values of W: $b = 4.4 \pm 0.3$ GeV^{-2} (H1) and $b = 4.6 \pm 0.6$ GeV^{-2} (ZEUS), as well as the ZEUS measurement [3] of $b = 5.1 \pm 1.3$ GeV^{-2} for $2 < Q^2 < 40$ GeV^2 and $55 < W < 125$ GeV.

In order to study a possible Q^2 or W dependence of the slope parameter, the data sample was divided in two bins in Q^2 and W, respectively, and the fitting procedure was repeated. With the present statistics no significant dependence of the b-parameter on W is found (see Table 2); there is however an indication for a decrease of b with Q^2.

4.3 Decay angular distributions for quasi-elastic J/ψ production

In order to investigate the helicity structure of J/ψ meson production [42] the angular distributions of the decay leptons in the helicity frame are used. In this frame, the J/ψ direction in the $\gamma^* p$ centre of mass system serves as the quantisation axis. Three angles are defined: the polar (θ^*) and azimuthal (φ) angles of the positive decay lepton in the J/ψ rest frame. The third angle is the angle ϕ between the normals to the J/ψ production plane (defined by the J/ψ and the scattered proton) and the electron scattering plane in the $\gamma^* p$ centre of mass system.

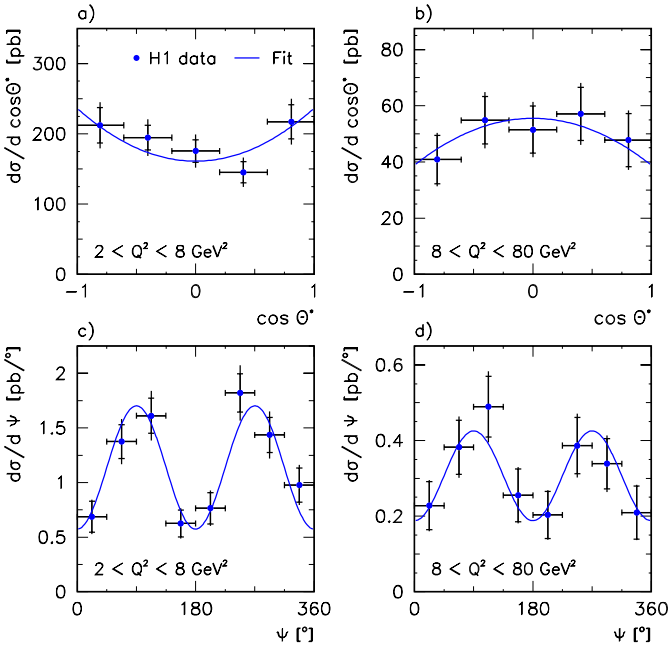

Fig. 9a–d. Angular distributions for the positive J/ψ decay lepton in quasi-elastic production processes $e+p \to e+J/\psi+X$ with $40 < W < 160$ GeV. **a** $\cos\theta^*$ for $2 < Q^2 < 8$ GeV^2 and **b** for $8 < Q^2 < 80$ GeV^2; **c** and **d** the polarization angle Ψ in the same Q^2 regions. The inner error bars indicate the statistical errors, while the outer bars show the statistical and systematic uncertainties added in quadrature. The lines are fits to the data as described in the text

The one-dimensional distributions in $\cos\theta^*$ and the polarization angle $\Psi = \varphi - \phi$ are extracted. If the helicity of the virtual photon is retained by the J/ψ meson (s-channel helicity conservation hypothesis, SCHC), the full angular distribution is a function of $\cos\theta^*$ and Ψ only.

The acceptance corrected $\cos\theta^*$ and Ψ distributions are shown in Fig. 9. Both the forward tagged and untagged event samples are used, since the helicity structure is expected to be independent of whether the proton dissociates or not, a hypothesis supported by the data. The $\cos\theta^*$ distribution is related to the spin density matrix element r^{04}_{00}, the probability of the J/ψ meson to be longitudinally polarized, according to

$$\frac{\mathrm{d}\,\sigma}{\mathrm{d}\,\cos\theta^*} \propto 1 + r^{04}_{00} + (1 - 3r^{04}_{00})\cos^2\theta^*. \qquad (10)$$

A χ^2 fit to the data shown in Figs. 9a and b yields, for an average $\langle W\rangle = 96$ GeV:

$$r^{04}_{00} = 0.15 \pm 0.11 \quad \text{for} \quad \langle Q^2\rangle = 4 \text{ GeV}^2, \qquad (11)$$
$$r^{04}_{00} = 0.48 \pm 0.15 \quad \text{for} \quad \langle Q^2\rangle = 16 \text{ GeV}^2. \qquad (12)$$

The Ψ distribution is related to the spin density matrix element r^1_{1-1}:

$$\frac{\mathrm{d}\,\sigma}{\mathrm{d}\,\Psi} \propto 1 - \varepsilon\, r^1_{1-1}\cos 2\Psi. \qquad (13)$$

A fit to the data shown in Figs. 9c and d yields

$$r^1_{1-1} = 0.50 \pm 0.08 \quad \text{for} \quad \langle Q^2\rangle = 4 \text{ GeV}^2, \qquad (14)$$
$$r^1_{1-1} = 0.39 \pm 0.13 \quad \text{for} \quad \langle Q^2\rangle = 16 \text{ GeV}^2. \qquad (15)$$

In the case of s-channel helicity conservation and natural parity exchange (NPE) the matrix elements r^{04}_{00} and r^1_{1-1} are related by $r^1_{1-1} = \frac{1}{2}(1 - r^{04}_{00})$. Using this relation and the measured values for r^{04}_{00}, one obtains values for r^1_{1-1} which agree to within one standard deviation with those obtained from the Ψ angular distributions, thus supporting the SCHC and NPE hypotheses.

Under the assumption of SCHC the measurement of the r^{04}_{00} matrix element can be used for the determination of R, the ratio of the longitudinal to the transverse cross section:

$$R = \frac{\sigma_L}{\sigma_T} = \frac{1}{\varepsilon}\,\frac{r^{04}_{00}}{1 - r^{04}_{00}}. \qquad (16)$$

Using this relationship and the $\cos\theta^*$ distribution R is determined in two Q^2 regions:

$$R = 0.18^{+0.18}_{-0.14} \quad \text{for} \quad \langle Q^2\rangle = 4 \text{ GeV}^2 \quad \text{and} \qquad (17)$$
$$R = 0.94^{+0.79}_{-0.43} \quad \text{for} \quad \langle Q^2\rangle = 16 \text{ GeV}^2 \qquad (18)$$

with $\langle W\rangle = 96$ GeV. A measurement of $R = 0.41^{+0.45}_{-0.52}$ by the ZEUS experiment [3] at $\langle Q^2\rangle = 5.9$ GeV^2 and $\langle W\rangle = 97$ GeV is compatible with these values. Taking into account the photoproduction measurements of $R = 0.17 \pm 0.14$ [4] and $R = -0.01 \pm 0.09$ [5], which are compatible with the expectation $R = 0$ for $Q^2 = 0$, a rise of R with increasing Q^2 is suggested by the data.

The measured values of the R parameter are significantly smaller for J/ψ than for elastic ρ meson production at HERA [2,3,43] at similar Q^2; but they are of the same order if compared at the same value of Q^2/m_V^2, where m_V is the mass of the ρ or the J/ψ.

5 Quasi-elastic $\psi(2S)$ production

For the selection of $\psi(2S)$ mesons the decay channel $\psi(2S) \to J/\psi\,\pi^+\pi^-$, where the J/ψ decays either in two electrons or two muons, is used. In this case no separation between elastic and proton dissociation is attempted due to limited statistics. The goal is to derive the ratio of cross sections for J/ψ and $\psi(2S)$ production as a function of Q^2. The lower Q^2 cut is reduced to 1 GeV^2 since the Q^2 dependent acceptance corrections cancel almost completely in the cross section ratio.

The signals in the quasi-elastic $\psi(2S)$ selection are displayed in Fig. 10. For the determination of the $\psi(2S)$ to J/ψ ratio the non-resonant background is subtracted using the sidebands of the di-lepton mass spectrum in the case of the J/ψ meson and using the sidebands of the $\Delta m = m_{\psi(2S)} - m_\psi$ distribution for the $\psi(2S)$ meson. The data are divided in three Q^2 bins: $1 < Q^2 < 5$ GeV^2, $5 < Q^2 < 12$ GeV^2 and $12 < Q^2 < 80$ GeV^2. The cross

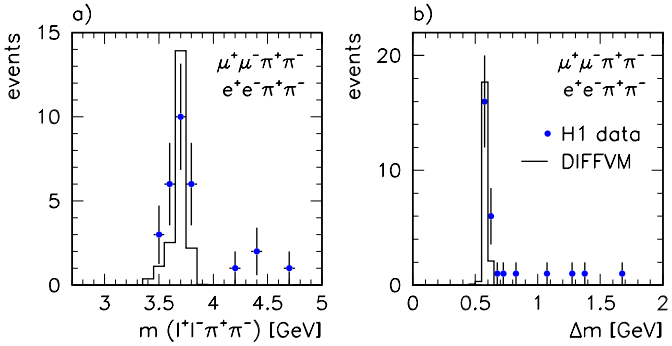

Fig. 10. a Mass spectrum of the four particles $\ell^+\ell^-\pi^+\pi^-$ and **b** $\Delta m = m_{\psi(2S)} - m_{\psi}$ for the $\psi(2S)$ candidate events, i.e. for events with $|m_{ll} - m_{\psi}| < 300$ MeV. The DIFFVM Monte Carlo simulations for the signals are shown for comparison

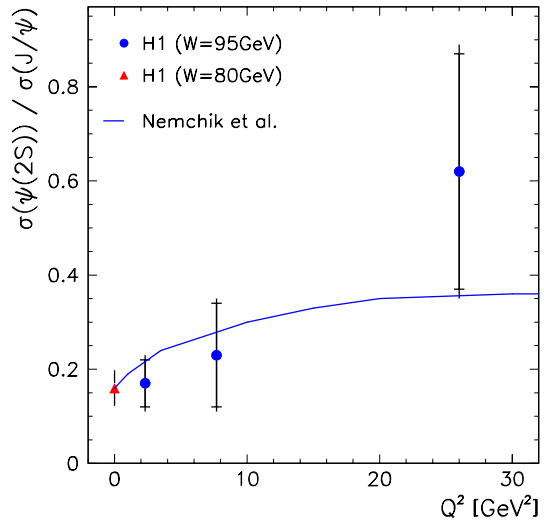

Fig. 11. Ratio of cross sections for the quasi-elastic production of $\psi(2S)$ and J/ψ mesons as a function of Q^2 for this analysis and for the H1 photoproduction measurement [44], corrected for the most recent branching fraction $BR(\psi(2S) \to J/\psi\,\pi^+\pi^-) = 30.2 \pm 1.9\%$ [28]. The inner error bars on the H1 points from this analysis indicate the statistical uncertainty, while the outer bars show the statistical and systematic uncertainties added in quadrature. The prediction from [11] based on colour dipole phenomenology is also displayed

section ratio is shown in Fig. 11. The systematic uncertainty of the ratio amounts to 16% in total and is dominated by the contribution from the track reconstruction efficiency for the low momentum $\pi^+\pi^-$ pair.

The measurement at low Q^2 agrees well with the H1 photoproduction measurement [44]. An indication of a rise with Q^2 at the level of two standard deviations is observed which is also predicted in models by Frankfurt et al. [8] and Nemchik et al. [11]. In [8] an asymptotic value of $\sigma_{\psi(2S)}/\sigma_{\psi} \approx 0.5$ is expected for $Q^2 \gg m_{\psi}^2$.

6 Inclusive and inelastic J/ψ production

Inclusive J/ψ production is studied in the kinematic range $2 < Q^2 < 80$ GeV^2 and $40 < W < 180$ GeV covering $0.2 < z \lesssim 1.0$ for the muonic decay of the J/ψ, while for the decay to electrons $z > 0.5$ is required. The restricted z region for $J/\psi \to e^+e^-$ is due to the smaller acceptance for electrons and larger background at low z values. The elasticity z (defined in Sect. 3.2) denotes the ratio of energies of the J/ψ and of the exchanged photon in the proton rest frame. Two sets of differential cross sections are determined. First an *inclusive* cross section is derived where in the given kinematic region all J/ψ mesons are selected irrespective of the production mechanism, thus including inelastic and elastic contributions. The inclusive cross sections are compared to the predictions of the Soft Colour Interaction Model [20]. A second set of differential cross sections is derived for *inelastic* J/ψ production which can be compared to the predictions within the NRQCD factorization approach [19] containing colour octet contributions.

An "inelastic" production process can be defined experimentally in several ways. In previous photoproduction analyses [4,14] cuts in the variable z, e.g. $z \lesssim 0.9$, were used to suppress elastic and proton dissociative events. In the present analysis a different approach is chosen because colour octet contributions are, in leading order in α_s, predominantly expected at large z. This is because the $c\bar{c}$ pair can be produced with no other particles in the final state, i.e. $z \sim 1$ (see Fig. 1e). Its non-perturbative evolution into the J/ψ meson reduces the value of z only slightly, and applying a z cut as done previously would reduce the expected colour octet contributions together with the quasi-elastic ones by an unknown amount. In the present analysis a cross section is determined suppressing contributions of low mass M_X following a suggestion of [19]. This suppression of low masses is achieved indirectly by requiring a minimal calorimetric energy in the forward region of the detector. This requirement selects high masses and suppresses elastic and proton dissociative events characterised by small M_X corresponding to small energy deposits in the forward direction. Colour octet contributions are expected to have $M_X \gtrsim 15$ GeV [19] and are retained.

6.1 Data analysis

The selection criteria as described in Table 1 are used. The di-lepton mass spectra of the selected events are shown in Fig. 12 separately for $0.2 < z < 0.6$ and $0.6 < z \lesssim 1$, both for the inclusive and the inelastic selection ($E_{fwd} > 5$ GeV). Since the non-resonant background increases with decreasing z the background fraction is determined from the mass spectra in bins of z by fitting the signal and background as in section 4. For the determination of the differential cross sections a correction is applied according to the z values of the events.

Acceptance and efficiencies are determined using a simulation tailored to describe the data, which consists of a

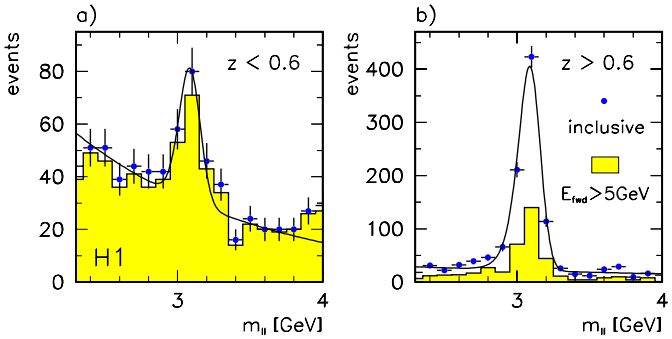

Fig. 12a,b. Di-lepton mass spectra for events of the inclusive (points) and inelastic (histogram) J/ψ selection: **a** $0.2 < z < 0.6$, **b** $0.6 < z \lesssim 1$. The curves are the results of fits of Gaussian distributions for the signal (convoluted with an exponential tail to account for energy loss in the case of di-electron decays) and an exponential distribution for the non-resonant background

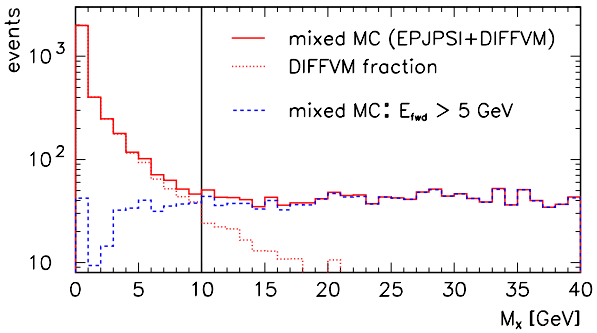

Fig. 14. Distribution of simulated J/ψ events as a function of the generated value of the mass M_X. The mixed Monte Carlo sample (DIFFVM and EPJPSI) is shown before (full histogram) and after (dashed histogram) applying the cut $E_{fwd} > 5$ GeV. The diffractive contribution as simulated by DIFFVM before the cut is also shown (dotted histogram)

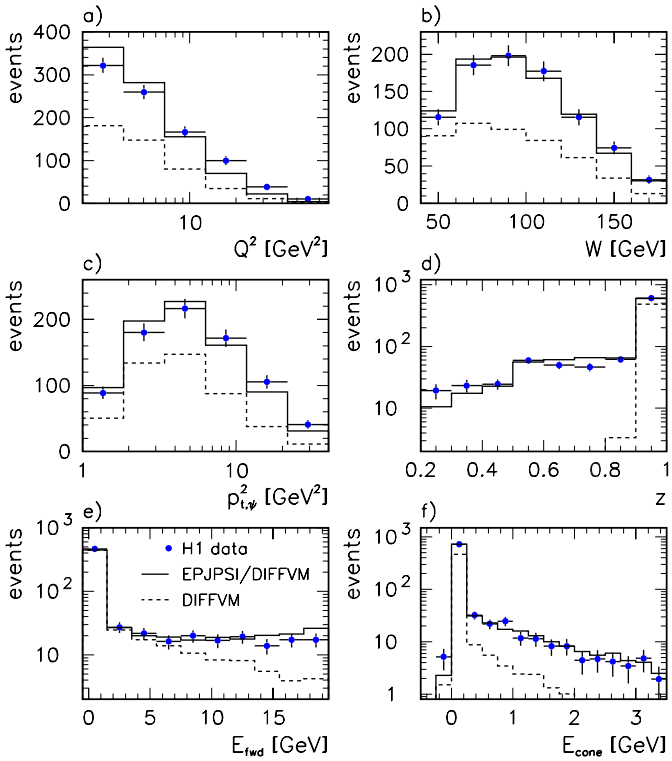

Fig. 13a–f. Comparison between data and Monte Carlo simulations for inclusive J/ψ production after all selection cuts in Table 1 and after background subtraction. Shown are distributions of **a** Q^2, **b** W, **c** the square of the J/ψ transverse momentum in the laboratory frame $p^2_{t,\psi}$, **d** the elasticity z, **e** the energy E_{fwd} deposited in the LAr calorimeter for $\theta < 20°$, and **f** the energy E_{cone} in a cone with radius $R = \sqrt{(\Delta\eta)^2 + (\Delta\phi)^2} = 1$ ($\eta = -\ln\tan(\theta/2)$) around the J/ψ direction of flight. The results of the combined Monte Carlo simulation (DIFFVM and EPJPSI, full lines) and of the DIFFVM simulation only (dashed lines) are shown. The error bars on the data points are statistical only

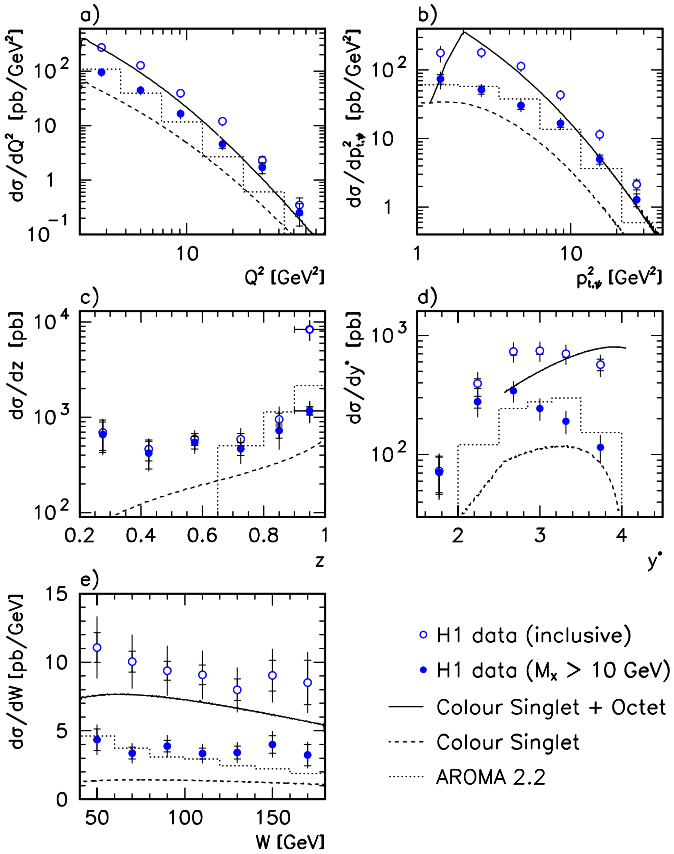

Fig. 15a–e. Differential cross sections for the inclusive (open points) and inelastic ($M_X > 10$ GeV, black points) $ep \to e\, J/\psi\, X$ process. **a** $d\sigma/dQ^2$, **b** $d\sigma/dp^2_{t,\psi}$ (see also footnote 8 concerning the theoretical prediction), **c** $d\sigma/dz$, **d** $d\sigma/dy^*$ and e) $d\sigma/dW$. The kinematic region is $2 < Q^2 < 80$ GeV^2, $40 < W < 180$ GeV and $z > 0.2$. The inner error bars are statistical, the outer error bars contain statistical and systematic uncertainties added in quadrature. The dotted histogram gives the prediction from the SCI model in AROMA 2.2 [21, 45] for inclusive J/ψ production. The curves are predictions for inelastic J/ψ production within the NRQCD factorization approach [19] for the colour singlet contribution (dashed line) and the sum of singlet and octet contributions (full line)

mix of diffractive events generated by DIFFVM [33] and of inelastic events generated by EPJPSI [36]. The diffractive events are composed of elastic and proton dissociative contributions in a ratio consistent with the signals observed in the forward detectors (compare Sect. 4). EPJPSI generates events according to the Colour Singlet Model. Both models were previously shown to describe quasi-elastic and inelastic data respectively (see for example [4]). Contributions from other processes such as b-decays or the hadronic component of the photon are expected to contribute only for $z \lesssim 0.4$ and are estimated to be negligible.

The EPJPSI contribution is normalized to the data in the interval $0.4 < z < 0.8$ and the DIFFVM contribution is added to describe the data in the region $z > 0.95$ (compare also Fig. 13d). Numerous checks were carried out to ensure that all important aspects of the data are well described by this mix. Comparisons between the data and the Monte Carlo simulation are shown in Fig. 13.

The systematic errors in this analysis are typically 18% and are dominated by uncertainties in the acceptance corrections, mainly due to the model uncertainty of the Monte Carlo description, the subtraction of non-resonant background, and reconstruction efficiencies. The largest systematic uncertainty (up to 32%) is found for large z and small $p^2_{t,\psi}$ values.

In a second step inelastic cross sections are determined for events with a large energy deposition in the forward region of the LAr calorimeter, namely $E_{fwd} > 5$ GeV for polar angles $\theta < 20^\circ$. This requirement is an indirect cut on the mass of the hadronic system X. Its effect can be seen for simulated events in Fig. 14 where the M_X distribution is shown for the mixed simulation (EPJPSI+DIFFVM) and for the fraction of the diffractive simulation (DIFFVM) separately. The latter dominates at low values of M_X and is suppressed efficiently by the cut on E_{fwd}. The differential cross sections for $M_X > 10$ GeV are thus determined by applying the cut $E_{fwd} > 5$ GeV and then correcting to $M_X > 10$ GeV using the Monte Carlo simulation.

6.2 Differential cross sections

Inclusive cross sections and soft colour interactions. Differential ep cross sections for inclusive J/ψ production are given in Table 6 and shown in Fig. 15 (open points) as functions of Q^2, $p^2_{t,\psi}$, z, y^* (the rapidity of the J/ψ in the $\gamma^* p$ centre of mass system) and W. The prediction of the Soft Colour Interaction Model (dotted histogram in Fig. 15) which is computed using a modified version of AROMA [21,45][6], is compared to the data. Although the model gives a reasonable description of the shapes of several distributions, there are major discrepancies in the z distribution and in the absolute values of the measured and predicted cross sections. For small z, the SCI model as implemented in AROMA is expected to fall below the data due to the missing hard contributions of the Colour Singlet Model which should also be taken into account [45]. At large z the AROMA SCI prediction is below the measured cross section by approximately a factor of four.

Inelastic cross sections and NRQCD factorization approach. The differential cross sections for inelastic J/ψ production, that is for $M_X > 10$ GeV, are also displayed in Fig. 15 (full points). In comparison with the inclusive cross sections the effect of requiring a high mass is most significant in the shapes of the distributions of z and y^*.

The results of the calculations by Fleming and Mehen [19] who applied the NRQCD factorization approach to electroproduction of J/ψ mesons are shown in Fig. 15 for comparison. The predicted cross sections include the contributions from the colour octet states $^3P_0$, $^1S_0$ which are of order $\mathcal{O}(\alpha_s)$ and the colour singlet state $^3S_1$ (of order $\mathcal{O}(\alpha_s^2)$)[7]. The sum of these contributions shown in Fig. 15 is computed using GRV(LO) [40] parton densities; the colour singlet contribution is also shown separately. Note that these predictions are for $c\bar{c}$ pairs from the hard subprocess and do not include any hadronisation effects. The hadronisation of the colour octet $c\bar{c}$ pairs into a colour singlet J/ψ is believed to proceed via emission of soft gluons[8].

The colour octet contribution dominates the cross section for all Q^2 (Fig. 15a). The colour singlet contribution (dashed curves in Fig. 15) is seen to fall below the data by factors $2-3$ while the prediction for the sum (full curves in Fig. 15) is overall too large in absolute magnitude by up to a factor 3. The shapes of the data distributions are not well reproduced by the calculation: the predicted Q^2 and $p^2_{t,\psi}$ distributions are steeper than the data and the y^* distribution increases towards larger values of y^* instead of falling. The W distribution agrees in shape but overshoots the data. The full prediction of the z distribution is at present not calculable [19] and is therefore not shown.

The observed differences in magnitude between the predicted and measured cross sections probably call for an overall adjustment of the fitted transition matrix elements while the shapes may be influenced by a relative adjustment of the individual contributions. There is a hint that these differences increase towards low Q^2 (see Fig. 15a, full points and full curve). The theoretical predictions are also expected to be more precise for larger Q^2 and $p^2_{t,\psi}$ [19]. Therefore the comparison was repeated for

[6] The following parameters are used in addition to standard settings: charm mass $m_c = 1.4$ GeV, GRV(HO) parton densities and $R = 0.5$, where R parameterizes the probability of a colour exchange between partons

[7] Spectroscopic notation is used: $^{2S+1}L_J$ where S, L and J denote spin, orbital and total angular momentum of the $c\bar{c}$ system that is produced in the hard process. The following values for non-perturbative long range transition matrix elements are used: $\langle \mathcal{O}^{J/\psi}_{(1)}(^3S_1)\rangle = 1.1$ GeV^3, $\langle \mathcal{O}^{J/\psi}_{(8)}(^1S_0)\rangle = 0.01$ GeV^3, and $\langle \mathcal{O}^{J/\psi}_{(8)}(^3P_0)\rangle/m_c^2 = 0.005$ GeV^3. The octet matrix elements $\langle \mathcal{O}^{J/\psi}_{(8)}\rangle$ were estimated from fits to the CDF data performed in [46] while the singlet matrix element is calculated from the measured electronic decay width of the J/ψ

[8] The sharp edge observed in Fig. 15b in the theoretical $p^2_{t,\psi}$ curve is a consequence of the missing hadronisation

Table 6. Inclusive and inelastic ($M_X > 10\,\mathrm{GeV}$) differential cross sections for the process $ep \to e\,J/\psi\,X$ in the kinematic region $2 < Q^2 < 80$ GeV^2, $40 < W < 180$ GeV and $z > 0.2$

Q^2		$\mathrm{d}\,\sigma(ep \to eJ/\psi X)/\mathrm{d}\,Q^2$			[pb/GeV^2]	
[GeV^2]		inclusive			$M_X > 10$ GeV	
2.8	269	± 16 (stat.)	± 43 (syst.)	95.5	± 8.8 (stat.)	± 15.3 (syst.)
5.0	127	± 8	± 20	44.4	± 4.3	± 7.1
9.1	39.5	± 3.2	± 6.3	16.4	± 2.0	± 2.6
17.1	12.0	± 1.3	± 1.9	4.5	± 0.7	± 0.7
31.1	2.28	± 0.40	± 0.36	1.69	± 0.37	± 0.27
54.5	0.35	± 0.12	± 0.06	0.25	± 0.11	± 0.04
$p^2_{t,\psi}$		$\mathrm{d}\,\sigma(ep \to eJ/\psi X)/\mathrm{d}\,p^2_{t,\psi}$			[pb/GeV^2]	
[GeV^2]		inclusive			$M_X > 10$ GeV	
1.4	177	± 20 (stat.)	± 44 (syst.)	73.7	± 11.6 (stat.)	± 18.4 (syst.)
2.6	180	± 14	± 29	51.4	± 7.0	± 8.2
4.8	114	± 8	± 18	30.5	± 3.8	± 4.9
8.6	43.4	± 3.5	± 6.9	16.7	± 2.1	± 2.7
15.5	11.5	± 1.2	± 1.8	5.0	± 0.7	± 0.8
27.0	2.14	± 0.35	± 0.34	1.28	± 0.27	± 0.20
z		$\mathrm{d}\,\sigma(ep \to eJ/\psi X)/\mathrm{d}\,z$			[pb]	
		inclusive			$M_X > 10$ GeV	
0.275	690	± 240 (stat.)	± 110 (syst.)	660	± 230 (stat.)	± 110 (syst.)
0.425	460	± 110	± 70	420	± 130	± 70
0.575	590	± 80	± 110	550	± 80	± 100
0.725	590	± 80	± 160	470	± 70	± 130
0.850	950	± 150	± 310	730	± 130	± 240
0.950	8350	± 390	± 2000	1170	± 110	± 280
y^*		$\mathrm{d}\,\sigma(ep \to eJ/\psi X)/\mathrm{d}\,y^*$			[pb]	
		inclusive			$M_X > 10$ GeV	
1.77	73	± 25 (stat.)	± 17 (syst.)	71	± 24 (stat.)	± 16 (syst.)
2.24	396	± 38	± 91	277	± 31	± 64
2.68	737	± 53	± 133	343	± 35	± 62
3.00	746	± 51	± 134	244	± 28	± 44
3.32	702	± 49	± 126	191	± 25	± 34
3.74	568	± 62	± 102	115	± 23	± 21
W		$\mathrm{d}\,\sigma(ep \to eJ/\psi X)/\mathrm{d}\,W$			[pb/GeV]	
[GeV]		inclusive			$M_X > 10$ GeV	
50	11.1	± 1.1 (stat.)	± 2.0 (syst.)	4.3	± 0.8 (stat.)	± 0.8 (syst.)
70	10.0	± 0.8	± 1.8	3.4	± 0.4	± 0.6
90	9.4	± 0.7	± 1.7	3.9	± 0.4	± 0.7
110	9.1	± 0.7	± 1.6	3.3	± 0.4	± 0.6
130	8.0	± 0.8	± 1.4	3.4	± 0.5	± 0.6
150	9.0	± 1.1	± 1.6	4.0	± 0.6	± 0.7
170	8.5	± 1.6	± 1.5	3.2	± 0.8	± 0.6

$Q^2 > 4$ GeV^2 and $p^2_{t,\psi} > 4$ GeV^2 (see Table 7), but no significant change in the conclusions was found.

6.3 Integrated cross sections and comparison with photoproduction

In Table 3 the integrated cross sections for $e + p \to e + J/\psi + X$ in the kinematic region $2 < Q^2 < 80$ GeV^2, $40 < W < 180$ GeV and $z > 0.2$ are summarised. They are given for the inclusive selection, for the inelastic selection corresponding to $M_X > 10$ GeV, and for $z < 0.9$ as in previous photoproduction analyses [4,14]. In addition, the cross sections after imposing the additional cuts $Q^2 > 4.0$ GeV^2 and $p^2_{t,\psi} > 4.0$ GeV^2 are provided.

The total cross section for $\gamma^* p \to J/\psi\,X$ is computed according to equation (7) as a function of the $\gamma^* p$ centre of

Table 7. Inclusive and inelastic ($M_X > 10\,\mathrm{GeV}$) differential cross sections for the process $ep \to e\,J/\psi\,X$ in the kinematic region $4 < Q^2 < 80\ \mathrm{GeV}^2$, $p^2_{t,\psi} > 4\ \mathrm{GeV}^2$, $40 < W < 180$ GeV and $z > 0.2$

z	$\mathrm{d}\,\sigma(ep \to eJ/\psi X)/\mathrm{d}\,z$ [pb]					
	inclusive			$M_X > 10$ GeV		
0.275	110	± 80 (stat.)	± 20 (syst.)	110	± 80 (stat.)	± 20 (syst.)
0.425	210	± 80	± 30	190	± 70	± 30
0.575	180	± 50	± 30	160	± 50	± 30
0.725	220	± 50	± 60	200	± 50	± 50
0.850	250	± 70	± 80	190	± 70	± 60
0.950	3750	± 240	± 900	530	± 70	± 130
y^*	$\mathrm{d}\,\sigma(ep \to eJ/\psi X)/\mathrm{d}\,y^*$ [pb]					
	inclusive			$M_X > 10$ GeV		
1.77	15	± 10 (stat.)	± 3 (syst.)	15	± 10 (stat.)	± 3 (syst.)
2.24	155	± 22	± 36	95	± 17	± 22
2.68	328	± 33	± 59	126	± 20	± 23
3.00	317	± 32	± 57	80	± 15	± 14
3.32	309	± 34	± 56	66	± 14	± 12
3.74	169	± 35	± 30	31	± 13	± 6
W [GeV]	$\mathrm{d}\,\sigma(ep \to eJ/\psi X)/\mathrm{d}\,W$ [pb/GeV]					
	inclusive			$M_X > 10$ GeV		
50	3.8	± 0.6 (stat.)	± 0.7 (syst.)	1.32	± 0.42 (stat.)	± 0.24 (syst.)
70	4.2	± 0.5	± 0.8	1.12	± 0.25	± 0.20
90	3.9	± 0.4	± 0.7	1.32	± 0.23	± 0.24
110	4.1	± 0.5	± 0.7	1.30	± 0.24	± 0.23
130	3.2	± 0.5	± 0.6	1.12	± 0.25	± 0.20
150	3.5	± 0.6	± 0.6	1.63	± 0.35	± 0.29
170	2.1	± 0.6	± 0.4	0.80	± 0.33	± 0.14

Table 8. W dependence of the inclusive and the inelastic ($z < 0.9$) cross sections $\sigma(\gamma^* p \to J/\psi\,X)$ in the kinematic region $2 < Q^2 < 80\ \mathrm{GeV}^2$, $40 < W < 180$ GeV and $z > 0.2$

W [GeV]	$\sigma(\gamma^* p \to J/\psi X)$ [nb]					
	inclusive			$z < 0.9$		
50	33.0	± 3.2 (stat.)	± 5.9 (syst.)	16.0	± 3.2 (stat.)	± 2.9 (syst.)
70	43.1	± 3.3	± 7.8	12.9	± 1.9	± 2.3
90	53.8	± 4.0	± 9.7	17.7	± 2.3	± 3.2
110	66.3	± 5.2	± 11.9	22.1	± 3.1	± 4.0
130	72.8	± 7.1	± 13.1	28.0	± 4.5	± 5.0
150	101	± 12	± 18	33.6	± 6.0	± 6.0
170	115	± 22	± 21	27.9	± 7.2	± 5.0

mass energy W at $\langle Q^2 \rangle = 9\ \mathrm{GeV}^2$ and is given in Fig. 16 and Table 8. The cross section is determined for the inclusive data $0.2 < z \lesssim 1$ and, in view of a comparison with photoproduction, also for an inelastic selection using a cut $z < 0.9$ [9]. The W dependence is seen to be very similar to that in the photoproduction data [4,14] also shown in Fig. 16. The W dependence, parameterized as W^δ, yields $\delta = 0.95 \pm 0.11$ for the inclusive data and $\delta = 0.89 \pm 0.20$ for the data with $z < 0.9$. The photoproduction data, including H1 and ZEUS, are described by $\delta = 0.91 \pm 0.26$. The errors include statistical and systematic uncertainties.

6.4 Decay angular distributions

Measuring the polarization of the J/ψ is thought to be a way of distinguishing the various contributions to J/ψ production. The polar (θ^*) decay angular distributions in the helicity frame are shown in Fig. 17 for the fully in-

[9] The photoproduction data are given for $0 < z < 0.9$. This was achieved by an extrapolation to $z = 0$ assuming contributions from photon gluon fusion only. This contribution at small z is however negligible in the comparison

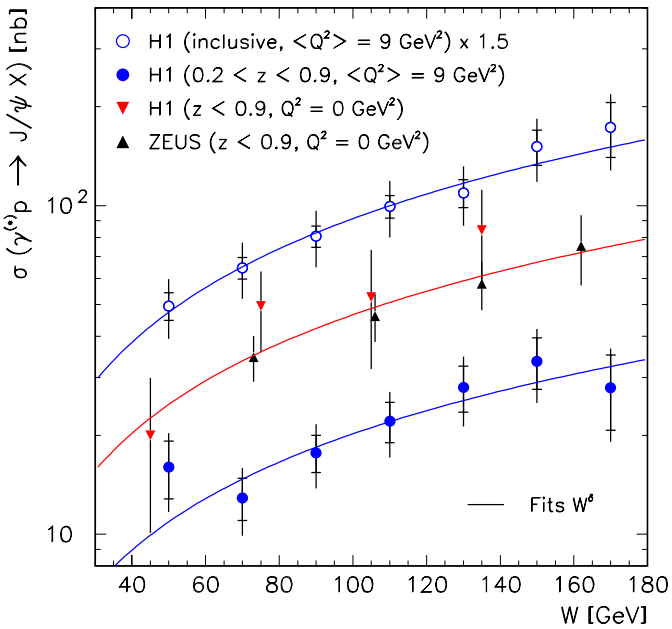

Fig. 16. Total cross sections for $\gamma^* p \to J/\psi\, X$ from this analysis at $\langle Q^2 \rangle = 9\ \mathrm{GeV}^2$. The inclusive cross section ($0.2 < z \lesssim 1.0$) is shown as a function of W (multiplied by a factor 1.5 for clarity), as well as the cross section for $0.2 < z < 0.9$. Photoproduction data [4,14] with similar cuts in z are included for comparison. The inner error bars on the points from this analysis indicate the statistical uncertainty, while the outer bars show the statistical and systematic uncertainties added in quadrature

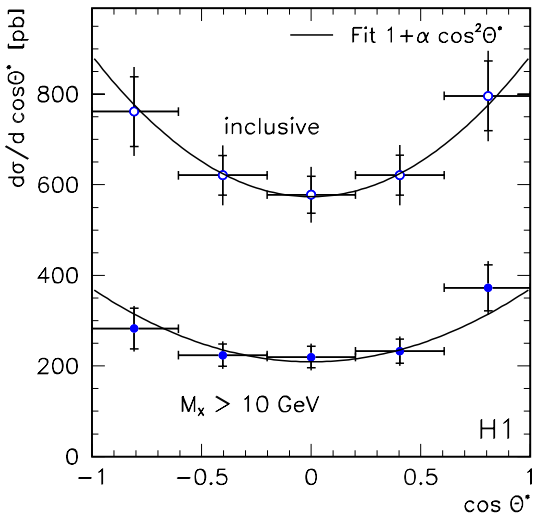

Fig. 17. Differential cross sections $d\sigma/d\cos\theta^*$ for $ep \to e\, J/\psi\, X$ in the kinematic region $2 < Q^2 < 80\ \mathrm{GeV}^2$, $40 < W < 180$ GeV and $z > 0.2$. The inclusive cross section and the inelastic cross section ($M_X > 10$ GeV) are shown. The inner error bars indicate the statistical uncertainty, while the outer bars include the statistical and systematic uncertainties added in quadrature. The lines are fits to the form $\sim 1 + \alpha \cos^2\theta^*$

clusive case and for the inelastic selection $M_X > 10$ GeV, in the kinematic region $2 < Q^2 < 80\ \mathrm{GeV}^2$, $40 < W < 180$ GeV and $z > 0.2$.

The $\cos\theta^*$ distribution is predicted to have the form

$$\frac{\mathrm{d}\,\sigma}{\mathrm{d}\,\cos\theta^*} \propto 1 + \alpha\,\cos^2\theta^*. \qquad (19)$$

For J/ψ production via the colour singlet mechanism $\alpha \approx 0.5$ is expected for the kinematic range studied here [47]. If colour octet contributions are present, $|\alpha| \lesssim 0.5$ is expected, where α can be negative, zero or positive depending on which intermediate $c\bar{c}$ state dominates the production [19].

The data yield values of $\alpha = 0.54^{+0.29}_{-0.26}$ for the inclusive case and $\alpha = 0.77^{+0.44}_{-0.38}$ for the inelastic selection ($M_X > 10$ GeV), including statistical and systematic uncertainties. The uncertainties are too large to draw definite conclusions.

7 Summary and conclusions

Measurements of elastic J/ψ production in deep inelastic scattering (DIS) with $25 < W < 160$ GeV and $2 < Q^2 < 80\ \mathrm{GeV}^2$ have been presented. They are more precise and cover a larger kinematic range than previous analyses at HERA. The dependence of the cross section $\sigma(\gamma^* p \to J/\psi\, p)$ on W is found to be proportional to W^δ with $\delta \simeq 1$, as was also observed in photoproduction. The Q^2 dependence is measured to be $\propto 1/(Q^2 + m_\psi^2)^n$ with $n = 2.38 \pm 0.11$. Both the W and Q^2 dependence are well described by a model based on perturbative QCD.

Assuming that the t dependence of elastic J/ψ production can be described by one exponential distribution, the slope parameter is determined to be $b = 4.1 \pm 0.3$ (stat.) $\pm$ 0.4 (syst.) GeV^{-2}, compatible with the value found in photoproduction. The helicity structure of quasi-elastic J/ψ production in DIS has been investigated and no evidence is found for a violation of s-channel helicity conservation. Assuming SCHC the ratio R of the longitudinal to the transverse cross section has been determined using the $\cos\theta^*$ distribution in two Q^2 regimes; the result is $R = 0.18^{+0.18}_{-0.14}$ for $\langle Q^2 \rangle = 4\ \mathrm{GeV}^2$ and $R = 0.94^{+0.79}_{-0.43}$ for $\langle Q^2 \rangle = 16\ \mathrm{GeV}^2$, suggesting a rise with Q^2.

The first evidence from HERA for quasi-elastic production of $\psi(2S)$ mesons in DIS has been reported. The increase of the ratio of cross sections for $\psi(2S)$ and J/ψ production with Q^2 predicted by models is supported by the data.

Data have been presented for the inclusive production of J/ψ mesons in deep inelastic scattering, covering the kinematic region $40 < W < 180$ GeV, $2 < Q^2 < 80\ \mathrm{GeV}^2$ and $0.2 < z \lesssim 1$. Differential ep cross sections are computed as functions of Q^2, $p^2_{t,\psi}$, z, y^* and W. The model of Soft Colour Interactions, a non-perturbative phenomenological approach to the description of inclusive J/ψ production, is compared to the data. The dependences of the differential cross sections on several variables are reasonably well described by the model, but the normalisations and the z dependence are not reproduced.

Using a selection cut designed to reject events with a low mass hadronic system, diffractive events are suppressed and inelastic cross sections ($M_X > 10$ GeV) are extracted. A leading order calculation in the NRQCD factorization approach using long range matrix elements determined from J/ψ production in $p\bar{p}$ collisions at the Tevatron is confronted with our measurements of differential inelastic cross sections. The shape and magnitude of the differential distributions are not described by the theoretical prediction. The comparisons may indicate the need to decrease the size of the colour octet long distance matrix elements or to change the relative importance of the different colour octet contributions, and/or to include higher orders in the NRQCD perturbative expansion. The colour singlet contribution alone is below the data by factors 2−3.

Acknowledgements. We are grateful to the HERA machine group whose outstanding efforts made this experiment possible. We appreciate the immense effort of the engineers and technicians who constructed and maintained the detector. We thank the funding agencies for their financial support of the experiment. We wish to thank the DESY directorate for the support and hospitality extended to the non-DESY members of the collaboration. We thank S. Fleming, L. Frankfurt, W. Koepf, T. Mehen, J. Rathsman and M. Strikman for valuable discussions and for making their theoretical predictions available. This paper was submitted for publication very soon after the tragic and untimely death of the DESY Director Björn Wiik. We would like to record here our appreciation of and gratitude for the friendship, encouragement, and support which he gave at all times to the H1 experiment.

References

1. E.g. A.R. Clark et al., *Phys. Rev. Lett.* **43** (1979) 187 and *ibid.* **45** (1980) 2092;EMCColl., J.J. Aubert et al., *Nucl. Phys.* **B21** (1983) 1
2. H1 Coll., S. Aid et al., *Nucl. Phys.* **B468** (1996) 3
3. ZEUS Coll., J. Breitweg et al., *Eur. Phys. J.* **C6** (1999) 603
4. H1 Coll., S. Aid et al., *Nucl. Phys.* **B472** (1996) 3
5. ZEUS Coll., J. Breitweg et al., *Z. Phys.* **C75** (1997) 215
6. M.G. Ryskin, *Z. Phys.* **C57** (1993) 89;M.G. Ryskin et al., *Z. Phys.* **C76** (1997) 231
7. S.J. Brodsky et al., *Phys. Rev.* **D50** (1994) 3134
8. L. Frankfurt, W. Koepf and M. Strikman, *Phys. Rev.* **D54** (1996) 3194
9. L. Frankfurt, W. Koepf and M. Strikman, *Phys. Rev.* **D57** (1998) 512
10. H1 Coll., S. Aid et al., *Nucl. Phys.* **B470** (1996) 3;H1 Coll., C. Adloff et al., *Nucl. Phys.* **B545** (1999) 21;ZEUS Coll., J. Breitweg et al., *Eur. Phys. J.* **C7** (1999) 609
11. B.Z. Kopeliovich and B.G. Zakharov, *Phys. Rev.* **D44** (1991) 3466;B.Z. Kopeliovich et al., *Phys. Lett.* **B324** (1994) 469;J. Nemchik et al., *Phys. Lett.* **B341** (1994) 228;J. Nemchik et al., *J. Exp. Theor. Phys.* **86** (1998) 1054
12. NMC Coll., D. Allasia et al., *Phys. Lett.* **B258** (1991) 493;EMC Coll., J. Ashman et al., *Z. Phys.* **C56** (1992) 21
13. E.L. Berger and D. Jones, *Phys. Rev.* **D23** (1981) 1521;R. Baier and R. Rückl, *Phys. Lett.* **B102** (1981) 364; *Nucl. Phys.* **B201** (1982) 1; *Z. Phys.* **C19** (1983) 251
14. ZEUS Coll., J. Breitweg et al., *Z. Phys.* **C76** (1997) 599
15. M. Krämer, *Nucl. Phys.* **B459** (1996) 3
16. CDF Coll., F. Abe et al., *Phys. Rev. Lett.* **69** (1992) 3704; *ibid.* **79** (1997) 572;DØColl., S. Abachi et al., *Phys. Lett.* **B370** (1996) 239; *Phys. Rev. Lett.* **82** (1999) 35
17. G.T. Bodwin, E. Braaten and G.P. Lepage, *Phys. Rev.* **D51** (1995) 1125, Erratum *ibid.* **D55** (1997) 5853;E. Braaten and Y. Chen,*Phys. Rev.* **D54** (1996) 3216;W.E. Caswell and G.P. Lepage, *Phys. Lett.* **B167** (1986) 437
18. M. Krämer, *Int. J. Mod. Phys.* **A12** (1997) 3985;M. Beneke, M. Krämer and M. Vänttinen, *Phys. Rev.* **D57** (1998) 4258;compare also: B. Cano–Coloma and M.A. Sanchis–Lozano, *Nucl. Phys.* **B508** (1997) 753;K. Sridhar K., A.D. Martin and W.J. Stirling, *Phys. Lett.* **B438** (1998) 211;B.A. Kniehl and G. Kramer, *Eur. Phys. J.* **C6** (1999) 493
19. S. Fleming and T. Mehen, *Phys. Rev.* **D57** (1998) 1846
20. A. Edin, G. Ingelman and J. Rathsman, *Z. Phys.* **C75** (1997) 57
21. G. Ingelman, J. Rathsman and G.A. Schuler, *Comput. Phys. Commun.* **101** (1997) 135
22. A. Donnachie and P.V. Landshoff, *Phys. Lett.* **B296** (1992) 227
23. See e.g. A. Donnachie and P.V. Landshoff, *Phys. Lett.* **B437** (1998) 408;A. Capella et al., *Phys. Lett.* **B337** (1994) 358;E. Gotsman, E.M. Levin and U. Maor, *Phys. Lett.* **B347** (1995) 424; *ibid.* **B403** (1997) 120
24. E. Braaten and S. Fleming, *Phys. Rev. Lett.* **74** (1995) 3327
25. A. Edin, G. Ingelman and J. Rathsman, *Phys. Rev.* **D56** (1997) 7317
26. J. F. Amundson et al., *Phys. Lett.* **B372** (1997) 127
27. H1 Coll., I. Abt et al., *Nucl. Instrum. Meth.* **A386** (1997) 310 and 348
28. Particle Data Group, C. Caso et al., *Eur. Phys. J.* **C1** (1998) 1
29. A. Meyer, PhD Thesis, University Hamburg (1998), DESY Thesis **98-012**
30. H1 Coll., R.D. Appuhn et al., *Nucl. Instrum. Meth.* **A386** (1997) 397, *ibid.* **A374** (1996) 149
31. S. Bentvelsen, J. Engelen and P. Kooijman, in: Proc. of the Workshop on Physics at HERA, ed. W. Buchmüller and G. Ingelman, Hamburg (1992), Vol. 1, p. 23; K.C. Hoeger, *ibid.*, p. 43
32. U. Bassler and G. Bernardi, *Nucl. Instrum. Meth.* **A361** (1995) 197
33. B. List, Diploma Thesis, Techn. University Berlin, unpublished (1993)
34. T. Sjöstrand, *PYTHIA 5.7 and JETSET 7.4. Physics and Manual*, preprint CERN-TH.7112/93 (1993) (revised February 1994)
35. K. Goulianos, *Phys. Rep.* **101** (1983) 169
36. H. Jung, in: Proc. of the Workshop on Physics at HERA, ed. W. Buchmüller and G. Ingelman, Hamburg (1992), Vol. 3, p. 1488; H. Jung et al., *Z. Phys.* **C60** (1993) 721
37. S.P. Baranov et al., in: Proc. of the Workshop on Physics at HERA, ed. W. Buchmüller and G. Ingelman, Hamburg (1992), Vol.3, p. 1478
38. A. Arbuzov et al., *Comput. Phys. Commun.* **94** (1996) 128
39. L.N. Hand, *Phys. Rev.* **129** (1963) 1834;S. Frixione et al., *Phys. Lett.* **B319** (1993) 339
40. M. Glück, E. Reya and A. Vogt, *Z. Phys.* **C67** (1995) 433
41. A.D. Martin, R.G. Roberts and W.J. Stirling, *Phys. Lett.* **B387** (1996) 419

42. T.H. Bauer et al., *Rev. Mod. Phys.* **50** (1978) 261;K. Schilling and G. Wolf, *Nucl. Phys.* **B61** (1973) 381;J.G. Körner et al., *Nucl. Phys.* **B204** (1982) 6, Erratum *ibid.* **B213** (1983) 546;S.D. Holmes,W. Lee and J.E. Wiss, *Ann. Rev. Nucl. Part. Sci.* **35** (1986) 397
43. H1 Coll., C. Adloff et al., DESY Report **99-010** (1999), subm. to Eur. Phys. J. C
44. H1 Coll., C. Adloff et al., *Phys. Lett.* **B421** (1998) 385
45. J. Rathsman, private communication (1998)
46. M. Beneke and M. Krämer, *Phys. Rev.* **D55** (1997) 5269
47. S. Fleming, private communication (1997)